Construction and Building Materials xxx (xxxx) 124205

Contents lists available at ScienceDirect

Construction and Building Materials

journal homepage: www.elsevier.com/locate/conbuildmat

# Effect of steel slag and curing temperature on the improvement in technological properties of biomass bottom ash based alkali-activated materials

M.A. Gómez-Casero [a], L. Pérez-Villarejo [b, c], E. Castro [a, c], D. Eliche-Quesada [a, c, *]

[a] Department of Chemical, Environmental, and Materials Engineering, Higher Polytechnic School of Jaén, University of Jaén, Campus Las Lagunillas s/n, 23071 Jaén, Spain
[b] Department of Chemical, Environmental, and Materials Engineering, Higher Polytechnic School of Linares, University of Jaén, Campus Científico-Tecnológico, Cinturón Sur s/n, 23700 Linares (Jaén), Spain
[c] Center for Advanced Studies in Earth Sciences, Energy and Environment (CEACTEMA), University of Jaén, Campus Las Lagunillas, s/n, 23071 Jaén, Spain

ARTICLE INFO

*Article history:*
Received 14 April 2021
Received in revised form 26 June 2021
Accepted 8 July 2021

*Keywords:*
Biomass bottom ash
Steel slag
Curing temperature
Alkali-activated materials

ABSTRACT

In this research the effect of the incorporation of black steel slag (BSS) (25, 50 and 75 wt%) into biomass bottom ash (BBA) as precursor in the synthesis of alkali-activated materials was studied. The alkali-activated pastes were cured at two temperatures, 60 and 20 °C. Thermal curing at 60 °C produced an increase in mechanical properties at early curing ages obtaining similar properties at older ages of 90 days. The addition of up to 50 wt% of BSS resulted in alkali-activated cements with increased compressive and flexural strengths. The increase in mechanical properties could be due to the formation of a higher amount of calcium aluminosilicate gel (C-A-H-S) with respect to potassium aluminosilicate gel (K-A-H-S) or to the synergistic formation of C-K-A-S-H gel. Therefore, these specimens can be used as a binding material for concrete production to replace Portland cement, which can lead to significant environmental and socio-economic improvements by reducing $CO_2$ emissions and consumption of natural resources.



## 1. Introduction

The search of alternative materials to Portland cement has increased in recent decades. Interest has been growing due to the high environmental impact produced by the manufacture of cement in both obtaining of raw materials and intense energy-demanding industrial process. To avoid this, more environmentally friendly materials have emerged. Interesting results have been obtained by alkali-activated materials [1]. These materials can be used as cement and be applied in concrete and mortar. Two models of alkali activated bonding systems are established [2]. The first one is the activation of silicon and calcium rich raw materials (steel slag) with alkaline solution whose main reaction product is calcium silicate hydrate (CSH) gel. In the second alkaline activation model, silicon- and aluminium-rich precursors (metakaolin or F-class coal fly ash) are used with alkaline solutions, and the reaction products are 3D polymeric Si-O-Al chains. Davidovits named the second group "Geopolymer" as they have a polymeric structure [3,4].

Alkali-activated materials can develop good results in term of mechanical strength and durability [5], but they have different behaviours depending on the origin of the material. There are two groups of origin of raw materials for alkali-activated materials manufacturing: natural and artificial. As for natural sources, there are kaolin [6–8], clays [9], or zeolites [10]; and as artificial sources: various fly ash [11–13], slag furnace [1,14–17] or other industrial waste and by-products [18–21]. The use of these raw materials as a source of aluminosilicates represents a decrease in energy consumption as well as $CO_2$ emissions, along with making a better use of wastes that were otherwise destined to landfill.

Several researchers have used different types of ash: carbon coal [22,23], or biomass ash as corn stalk or cob [24], bamboo [25], rice husk [26] and other waste from vegetable pruning [1]. The composition of biomass ashes depends on several factors, closely related to the biomass used as raw material. These ashes have a large amount of crystalline phase, with presence of inorganic amorphous material and organic matter [27]. The biomass combustion process generates two main types of solid waste: bottom ash (the waste generated by the combination of fully or partially burnt material that is discharged into the grate) and fly ash from the air pollution control system. Fly ashes have been widely used as a precursor material in geopolymers [28]. However, bottom ashes have not yet been widely used. Although both ashes have the

* Corresponding author at: Department of Chemical, Environmental, and Materials Engineering, Higher Polytechnic School of Jaén, University of Jaén, Campus Las Lagunillas s/n, 23071 Jaén, Spain.
*E-mail address:* deliche@ujaen.es (D. Eliche-Quesada).

https://doi.org/10.1016/j.conbuildmat.2021.124205
0950-0618/

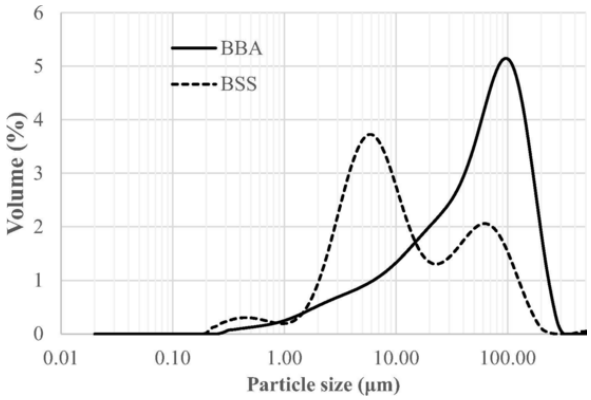


**Fig. 1.** Particle size distribution of precursors: BBA and BSS.

same origin, the composition could be different [29]. Bottom ashes have larger particle size and less glassy phase [30]. Some authors consider that fly ashes are more reactive than bottom ashes, and other authors say that the main differece is the particle size [31]. Thus, when larger bottom ash particles are crushed, higher surface area is achieved and reactivity of ashes are increased [29].

In alkaline environments, with higher pH values, reactive aluminosilicates present in the raw materials are rapidly dissolved [2,22]. In addition, high manufacturing temperature could help the dissolution of some compounds and accelerate the formation of geopolymeric gel. Therefore, the curing temperature is another condition that must be taken into account. Other authors have studied the effect of curing temperature on alkali-activated materials synthesis. Thus, Kaze et al. [32] studied the effect of temperature of curing on laterite-based geopolymer at 20, 60 and 80 °C. They obtained a raise of the dissolution of monomers and compressive strength at 7 and 28 days, when temperature was increased from 20 to 80 °C. Zribi et al. [33] studied the curing temperature of 60 °C and ambient temperature in the manufacture of phosphate-based alkali-activated materials. They found structural differences in the quantity of the phases formed and better compressive strength at high temperature. Zhang et al. [34] used several values of curing temperature and different material mixes. They obtained that increasing curing temperature results in better mechanical properties when glass powder was used. On slag-based alkali-activated cements adding waste glass, the optimal temperature was 80 °C, however on fly ash-based geopolymer the highest strength was obtained at 100 °C. Too high value of temperature can lead to decrease compressive strength. Tian et al. [35] showed the effect of a range of curing temperature (from 25 to 120 °C) of copper tailing-based alkali-activated materials and concluded that compressive strength decreased when curing temperatures above 80 °C were used. However, higher temperature has a high impact when specimens are manufactured with synthesis at room temperature having substantial advantages [33].

Black steel slag (BSS) is a by-product of steel production, from metallurgical industry. This waste is produced in steel making process, when molten steel and impurities are separated [36]. The main chemical components of BSS are Ca, Fe and Si. BSS has been used less in the construction industry, compared to ground granulated blast furnace slag [37]. Several researches were conducted by different researchers where steel slag (SS) was used as source of aluminosilicates and as aggregate to replace fly ash [38]. Song et al., [37] replaced fly ash by steel slag with differents percentage (range of 0–50 wt%). Replacing 20 wt% was the optimal ratio, without 28-day compressive strength loss. Besides, the setting times of the pastes were delayed with the incorporation of SS. Yazdi et al., [39] used ground granulated blast-furnace slag

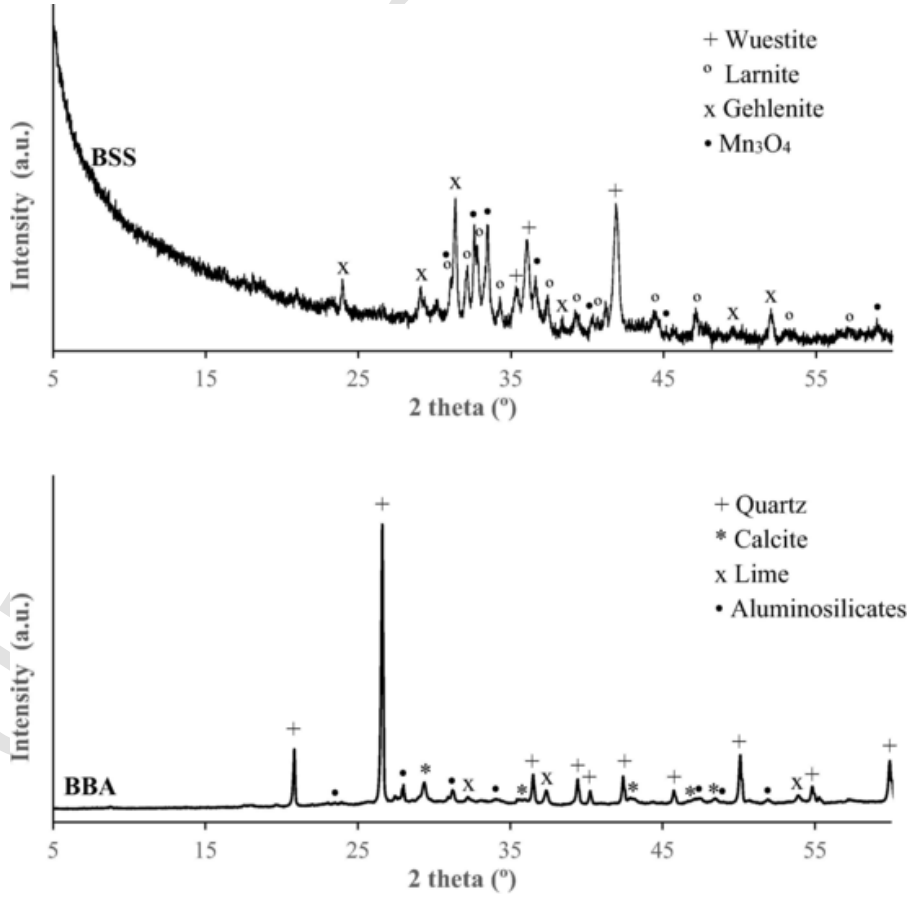


**Fig. 2.** XRD of precursors: BBA and BSS.

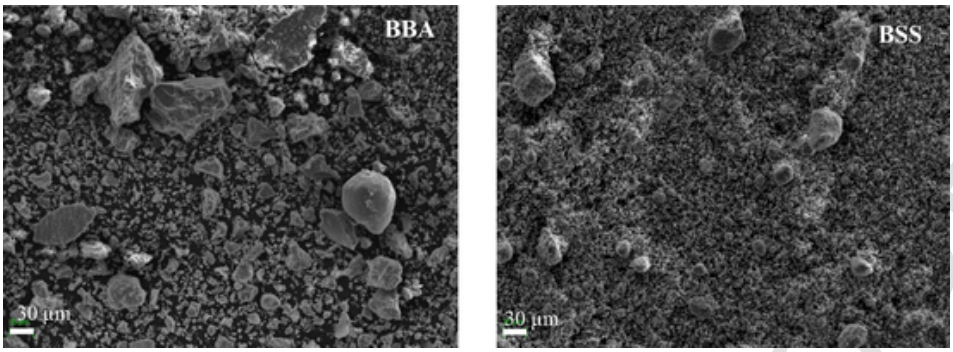


**Fig. 3.** SEM images and EDS analysis of precursors BBA and BSS.

**Table 1**
Chemical composition (wt. %) of the precursors.

| Raw material | $SiO_2$ | $Al_2O_3$ | $Fe_2O_3$ | CaO | MgO | MnO | $Na_2O$ | $K_2O$ | $TiO_2$ | $P_2O_5$ | $SO_3$ | LOI | HM | Kb |
|---|---|---|---|---|---|---|---|---|---|---|---|---|---|---|
| BBA | 46.10 | 12.04 | 4.78 | 19.65 | 3.71 | 0.09 | 0.78 | 4.59 | 0.83 | 1.12 | 0.41 | 5.58 | 0.77 | 0.40 |
| BSS | 17.29 | 10.71 | 24.16 | 30.89 | 2.63 | 5.68 | 0.16 | 0.03 | 0.79 | 0.41 | 0.28 | 5.39 | 2.56 | 1.20 |

to replace fly ash at 30 to 100 wt% cured on room temperature. They obtained high values of mechanical strength with the incorporation of up to 50 wt% slag, however when over 50 wt% of fly ash was replaced, compression strength did not increase, unlike flexural strength. In addition, other researchers achieved less curing time and better compressive strength when replacing fly ash by ground granulated blast-furnace slag [40,41]. The high CaO content in slag may help to form the C–S–H gel [40]. Using ashes can decrease water demand and allow paste workability times [41]. Nath and Kumar [42] also obtained similar results to ground granulate blast-furnace slag using granulated corex slag.

The addition of slag to biomass bottom ash has hardly been studied. Biomass bottom ashes have been used as a precursor to replace metakaolin in the manufacture of geopolymers. The optimal results were achieved with the incorporation of 50 wt% of waste [43]. The main aim of the work as the ashes are not very reactive, is to study the effect of 20 °C and thermal curing (60 °C), as well as, the addition of steel slags on the modification of the properties (physical properties: bulk density; mechanical properties: flexural and compressive strength and thermal properties: thermal conductivity) of biomass bottom ash-based alkali-activated control cements. The pastes were also characterized by X-ray diffraction (XRD), scanning electron microscopy (SEM) and Fourier transform infrared spectroscopy (FTIR). By adding slag to biomass bottom ash, authors try to develop room temperature cured binders. This could facilitate the manufacture of these materials, thus reducing the use of Portland cement and energy costs.

## 2. Materials and methods

### 2.1. Raw materials and characterization

The biomass bottom ash (BBA) was supplied by the Aldebarán Energía del Guadalquivir a power plant located in Andújar (Jaén, Spain). The plant uses biomass from olive pruning and biomass from forestry (forest biomass) and energy crops to generate renewable energy. The ashes have a heterogeneous particle size and are therefore ground and sieved to a grain size of less than 100 µm.

The black steel slag (BSS) comes from the Siderúrgica Sevillana S.A. industry located in San Juan de Aznalfarache (Seville, Spain).This industry belongs to the non-integral iron and steel sector, which valorises ferrous scrap to convert it into usable products such as steel bars of different profiles, diameters and qualities. Slag is produced in the electric arc furnace during the melting process of ferrous scrap. The slag has a grain size of 4–5 mm, which is why it must be crushed in a jaw crusher and ball mill and screened to a particle size of less than 100 µm. The particle size distribution of precursor, BBA and BSS was obtained by laser diffraction analysis using a Malvern Mastersizer 2000 laser diffractometer (Fig. 1). The BBA particles have a more homogeneous distribution and a higher mean particle size ($D_{50}$ = 52.6 µm) than the BSS particles with a more heterogeneous particle size distribution but with a slightly lower mean particle size ($D_{50}$ = 8.7 µm).

The crystalline mineralogical phases of the raw materials were identified by X-ray diffraction (XRD) with the Empyrean equipment with a PIXcel-3D detector from PANalytical using Cu K radiation (λ = 1.5406 Å) at a voltage of 40 kV and an amperage of 40 mA, a 2 theta range of 10 to 60 ° and a step size of 0.02. For phase identification, the HighScore software was used. In the BBA, silica ($SiO_2$) and calcium carbonate ($CaCO_3$) are identified as crystalline phases, presenting in smaller proportion calcium oxide (CaO), aluminosilicates $Al_{0.5}Ca_2Mg_{0.75}O_7Si_{1.75}$ and $Al_{0.83}Ca_{3.027}Fe_{1.17}O_{12}Si_3$ and silicoaluminates of Na and K. BSS present a more amorphous structure as indicated by the deviation from the baseline with diffraction peaks corresponding to wuestite (FeO), larnite ($Ca_2SiO_4$) and gehlenite ($Ca_2Al(SiAl)O_7$) with traces of manganese oxide ($Mn_3O_4$) (Fig. 2).

The micrographs of the raw materials (Fig. 3) were obtained by Scanning Electron Microscopy (SEM) using a JEAL model SM 840 assisted by Energy Dispersive X-ray spectroscopy (EDS). The precursors were placed on an aluminium grid and coated with carbon using the JEOL JFC 1100 sputter coater. Two types of particles can be observed in the BBA, spherical and irregular particles, while in the BSS waste only irregular particles are present. In both precursors, particles of different sizes can be observed. The particle size of the BBA being larger than that of the BSS.

The main chemical oxides in the precursors were identified by X-ray fluorescence (XRF) using a Philips Magix Pro model PW-2440 and are presented in Table 1. The major components of the BBA waste are $SiO_2$ (46.10%), CaO (19.65%) and $Al_2O_3$ (12.04%). Other oxides present in quantities close to 5 % are FeO, $K_2O$ and MgO. The BSS waste are mainly made up of CaO (30.89%), with a high percentage of $Fe_2O_3$ (24.16%), $SiO_2$ (17.29%) and $Al_2O_3$ (10.71%). In addition, present in smaller quantities are MnO (5.68 %) and MgO (2.63 %). The reactivity of a binder is governed by its oxide composition [44]. The modulus of hydration (HM) which represents the hydraulic activity of the binders and the coefficient of basicity (Kb) which is the ratio of basic oxides to acidic oxides were determined according to the equations (1) and (2) [45].

$$HM = \frac{CaO + Al_2O_3 + MgO}{SiO_2} \quad (1)$$

**Table 2**
Mix proportion.

| Sample | BBA (g) | BSS (g) | KOH (g) | $H_2O$ (g) | $K_2SiO_3$ (g) | l/s ratio | Curing Temperature (°C) | RH (%) |
|---|---|---|---|---|---|---|---|---|
| 100BBA-0BSS | 400 | 0 | 37.1 | 46.9 | 156 | 0.6 | 60 | 90 |
| | | | | | | | 20 | 90 |
| 75BBA-25BSS | 300 | 100 | 37.1 | 46.9 | 156 | 0.6 | 60 | 90 |
| | | | | | | | 20 | 90 |
| 50BBA-50BSS | 200 | 200 | 37.1 | 46.9 | 156 | 0.6 | 60 | 90 |
| | | | | | | | 20 | 90 |
| 25BBA-75BSS | 100 | 300 | 37.1 | 46.9 | 156 | 0.6 | 60 | 90 |
| | | | | | | | 20 | 90 |

$$Kb = \frac{(CaO + MgO)}{(SiO_2 + Al_2O_3)} \quad (2)$$

The BBA waste has a hydraulic modulus of 0.77 and a basicity coefficient of 0.40 significantly lower than BSS with hydraulic modulus and basicity coefficient of 2.56 and 1.20 respectively. These data indicate a higher reactivity of BSS and thus a beneficial effect of their incorporation into BBA, which could favour their hardening when curing at room temperature [46].

### 2.2. Preparation of alkali-activated cements

The possibility of using BBA as a precursor in the development of alkali-activated cements was evaluated. The modification of the properties of specimens with the incorporation of different amounts of BSS (25–75 wt%) was studied. Other authors have studied the incorporation of slags into fly ash based geopolymers to achieve room temperature curing. The high CaO content in slags accelerates the dissolution of materials and improves the properties of alkali-activated materials [47,48].

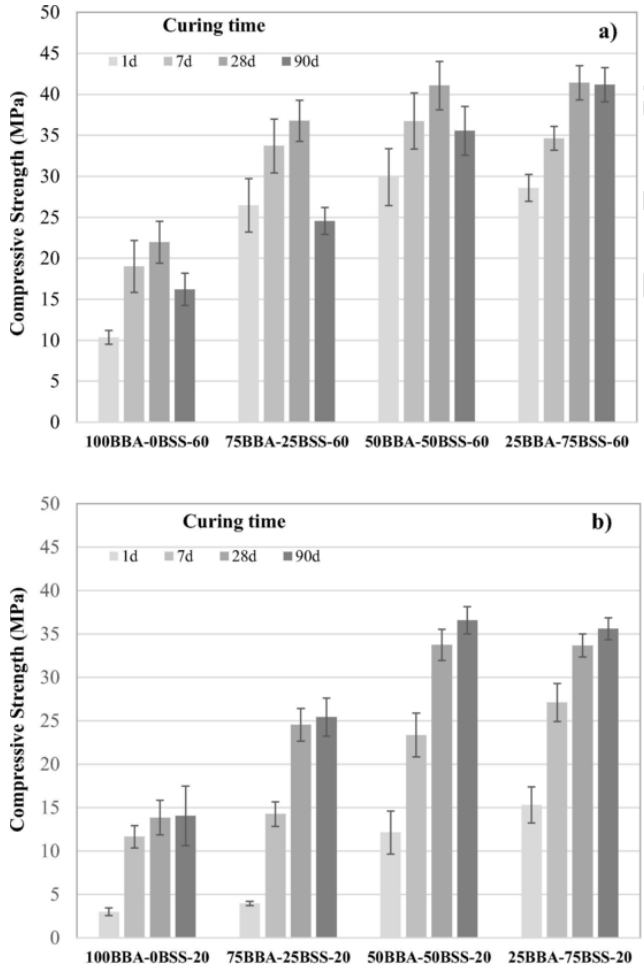


**Fig. 4.** Development of the compressive strength over time for alkali-activated cements with various BSS contents (a) heat curing at 60 °C for 24 h and (b) 20 °C.

The alkaline activator used is a solution of potassium hydroxide, 12 M KOH and potassium silicate. The potassium hydroxide was supplied by the company GlobalChem, and has a purity of 85%. The potassium silicate solution was supplied by the Roth company and has a composition by weight of 7.5–8.7% $K_2O$, 19.5–21.8% $SiO_2$ and 69.5–73% $H_2O$ and a density of 1.25 kg/l. Previous studies of the control alkali-activated cements were carried out using a silicate-hydroxide ratio of 65–35% (Ms = $SiO_2/Na_2O$ = 1.2) and different KOH concentrations (8, 12 and 15 M). The best compresive strength at 7 days was obtained for a concentration of 12 M KOH. Subsequently, different Ms (Ms = 0.75 silicate-hydroxide: 50–50 %; and Ms = 1.8, silicate-hidroxide: 75–25 %) were studied, obtaining the best compressive strengths at 7 days for the Ms = 1.2 (silicate-hidroxide ratio 65–35 %). Hence, the silicate-hydroxide (12 M) ratio used is 65–35 % with a silica modulus, Ms, of 1.2. After preparing the activating solution, it was cooled to room temperature and the pH was measured with a Crison Basic 20 pH meter. For all alkali-activated materials, the liquid/binder ratio selected was 0.6 in order to obtain adequate workability.

The mixtures of alkali-activated materials were prepared in a Proeti planetary mixer using the same sequence for all compositions. The dry raw materials, BBA and BSS, were mixed and homogenised for 90 s at low speed. After this time, the activator solution was added to the homogeneous mixture and mixed at low speed for another 90 s. Subsequently, the walls of the container were stirred and the mixture was mixed again for another 30 s at low speed. The workable paste obtained was poured into the 60x10x10 mm stainless steel moulds and subjected to 60 S on a Proeti shaking table to eliminate bubbles and achieve better compaction of the material. The moulded pastes were cured for 24 h in a climatic chamber Daihan ThermoStable STH-305 of 90 % relative humidity at 60 ± 1 °C or at 20 ± 1 °C, in order to study the effect of the curing temperature. Subsequently, the hardened pastes were demoulded and stored in a climatic chamber at 90 % relative humidity and 20 ± 1 °C until the curing age of 7, 28 and 90 days. Details of the ratio of the mixtures are presented in Table 2. The samples are designated as *x*BBA-*y*BSS-T-*t* where × is the BBA precursor content, *y* the BSS precursor content, T the curing temperature and *t* the curing time.

### 2.3. Experimental methods

The bulk density of the samples was measured according to the Archimedes principle following the standard UNE-EN 1015–10 [49] presenting the average of five determinations of each sample.

The specimens were subjected to flexural strength tests in accordance with UNE-EN 1015–11:2000/A1:2007 [50]. An MTS Insight 5 machine (5 kN capacity) with a displacement speed of 1.0 mm/min was used. In total, five samples of each composition and curing time were tested. The flexural strength ($\sigma_F$) was determined by the following equation:

$$\sigma_F = 1.5\frac{Fl}{bd^2} \quad (3)$$

where *F* is the load in newtons (N); *l* is the distance between the axes of the support rollers, in millimetres (mm); *b* is the width of the specimen, in millimetres (mm) and *d* is the thickness of the specimen, in millimetres (mm).

The mechanical compressive strength of five specimens was determined according to the UNE-EN105-11:2000/A1:2007 standard [50]. This test is carried out on the universal testing machine MTS 8101 (100 kN). The compressive strength is determined from equation (4).

**Table 3**
Degree of reaction of specimens, Si/Al, Ca/Si y Ca/Al molar ratio.

| Sample | Curing Temperature (°C) | Degree Reaction (%) | | | | |
|---|---|---|---|---|---|---|
| | | Curing time 1d | 28d | Si/Al | Ca/Si | Ca/Al |
| 100BBA-0BSS | 60 | 58.5 | 69.0 | 3.82 | 0.39 | 1.49 |
| | 20 | 51.3 | 64.0 | | | |
| 75BBA-25BSS | 60 | 76.5 | 80.0 | 3.41 | 0.51 | 1.75 |
| | 20 | 75.0 | 78.0 | | | |
| 50BBA-50BSS | 60 | 83.5 | 86.5 | 2.97 | 0.68 | 2.02 |
| | 20 | 82.6 | 85.0 | | | |
| 25BBA-75BSS | 60 | 94.0 | 95.0 | 2.50 | 0.92 | 2.31 |
| | 20 | 91.5 | 94.0 | | | |

$$\sigma_C = \frac{F}{S} \tag{4}$$

where $\sigma_c$ is the compressive strength (MPa); $F$ is the maximum ultimate load (N) and $S$ is the area of the specimen face under load ($mm^2$).

The thermal conductivity of two samples of 55 mm diameter and 15 mm thick specimens after 28 days of curing was determined according to ISO 8302 [51], using a FOX 50 TA instruments heat flow meter.

The degree of reaction, XRD, Attenuated Total Reflectance Fourier Transform Infrared Spectroscopy (ATR-FTIR) and SEM-EDS are the techniques used to determine the hydration products of the alkali-activated cements. To determine the degree of reaction of the hardened specimens, 1 g of ground and sieved sample (100 μm) was attacked with a HCl solution (1:20) [52]. The geopolymer gel formed is dissolved in the solution, which is then filtered, dried and calcined at 1000 °C (3 h). From the equation 5 the reaction degree is obtained:

$$Degree\ reaction\ (\%) = 1 - calcined\ mass * 100 \tag{5}$$

XRD analysis was applied to powder samples (≤100 μm) using the same equipment and operating conditions as for the raw materials. ATR-FTIR was performed using a Vertex 70 Bruker in the range 4000–400 $cm^{-1}$. The microstructural development of the hardened materials was obtained by SEM-EDS.

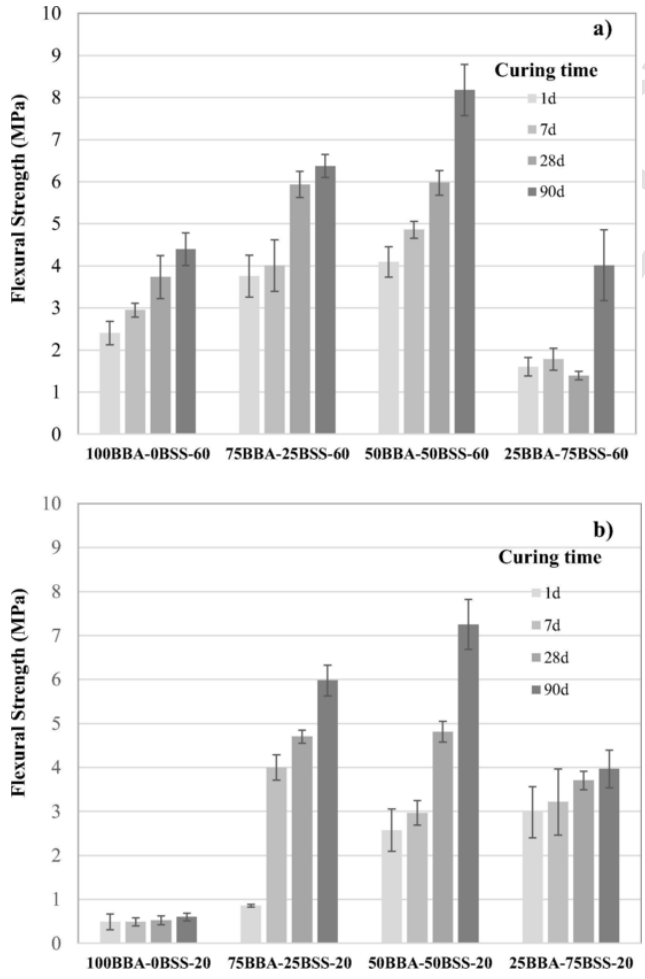


**Fig. 5.** Development of the flexual strength over time for BBA-BSS alkali-activated pastes (a) heat curing at 60 °C for 24 h and (b) 20 °C for 24 h.

## 3. Results and discussion

### 3.1. Compressive and flexural strengths

Compressive strength is one of the most important engineering properties for determining the use of new alkali-activated materials as structural construction material. The effect of curing temperature on the compressive strength of alkali-activated cements at different curing times, for different BBS contents is presented in Fig. 4. The compressive strength of specimens heat cured at 60 °C is higher than that of materials cured at 20 °C. Curing at higher temperatures in the first 24 h facilitated the development of mechanical strength. The increase in compressive strength at a curing temperature of 60 °C can be attributed to a high dissolution of the reactive species contained in the solid precursors at elevated temperatures leading to an increase in the reaction rate, resulting in a high degree of geopolymerization, as indicated by the higher values of the degree of reaction of the alkali-activated cements after 1 day of curing (Table 3) leading to a high polycondensation or polymerization between the Si, Al, Ca and Fe species. This suggests that the matrix was made more compact and denser by the initial curing at 60 °C, which justifies the high strength gained in these samples at low curing times with very little increase in compressive strength at longer curing times, especially in the binary alkali-activated cements containing BBA-BSS. The compressive strength of the control alkali-activated cements containing only BBA was 10.4 MPa and 3.0 MPa for a curing temperature of 60 and 20 °C, respectively for a curing time of 1 day. The compressive strength increased to 22.0 MPa and 13.8 MPa, respectively after 28 days of curing. Therefore, a higher increase in compressive strength with curing time can be observed for alkali-activated cements cured at 20 C°. A similar trend was observed in other studies where other aluminosilicate sources were used, concluding that increasing the curing temperature improves the mechanical properties of the aluminosilicates [32,53].

The addition of BSS resulted in a significant improvement of the compressive strength at both curing temperatures. For example, the 50BBA-50BSS-60 alkali-activated cements show compressive strengths at 1 day of cure of 29.9 MPa increasing to 41.1 MPa after 28 days of curing and to 37.2 MPa at 90 days of curing. The 50BBA-50BSS-20 samples reach 12.1, 33.7 and 36.6 MPa after 1, 28 and 90 days of curing. These data indicate that the incorporation of BSS into biomass ashes with low reactivity can be improved by incorporating a sufficient amount of BSS. The replacement of 50 wt% BSS improves the compressive strength and allows similar compressive strengths to be achieved at long curing times (90 days) regardless of whether curing takes place at 60 °C or at 20 °C. A proportion higher than 50 wt% BSS did not lead to an improvement in compressive strength. This fact has been observed by other authors [54]. Therefore, 50 wt% BSS can be considered as the optimum content that resulted in specimens with the highest compressive strength for both curing temperatures. The increase in compressive strength due to the incorporation of BSS is attributed to the development of alkaline aluminosilicate gel or geopolymer gel. The aluminosilicate gel formation is influenced by the chemical components of the precursors and the alkaline solution. It can be seen from Table 3 that as the BSS content increased, the Si/Al molar ratio of the mixtures de-

**Table 4**
Bulk density over time for alkali-activated cements with various BSS contents heat curing at 60 °C and 20 °C for 24 h.

| Sample | Curing T (°C) | Bulk density (kg/m³) Curing time | | | |
|---|---|---|---|---|---|
| | | 1d | 7d | 28d | 90d |
| 100BBA-0BSS | 60 | 1529 ± 27 | 1554 ± 34 | 1557 ± 5 | 1586 ± 23 |
| | 20 | 1411 ± 29 | 1437 ± 54 | 1446 ± 56 | 1454 ± 32 |
| 75BBA-25BSS | 60 | 1587 ± 5 | 1616 ± 2 | 1626 ± 2 | 1652 ± 20 |
| | 20 | 1512 ± 14 | 1523 ± 12 | 1544 ± 55 | 1552 ± 11 |
| 50BBA-50BSS | 60 | 1643 ± 14 | 1679 ± 9 | 1687 ± 17 | 1696 ± 34 |
| | 20 | 1545 ± 13 | 1553 ± 5 | 1581 ± 5 | 1596 ± 30 |
| 25BBA-75BSS | 60 | 1716 ± 54 | 1733 ± 12 | 1788 ± 53 | 1890 ± 28 |
| | 20 | 1565 ± 5 | 1581 ± 15 | 1634 ± 21 | 1663 ± 15 |

creased. The compressive strength of the alkali-activated cements increased with decreasing Si/Al molar ratio from 3.82 (100BBA-0BSS) to 2.96 (50BBA-50BSS). The silicate gel did not contribute significantly to the mechanical strength, the aluminosilicate gel being stronger [55]. The presence of a lower amount of Si in the BSS-containing alkali-activated cements made more $Al(OH)_4^{-4}$ species available for condensation in the early stages of curing. In addition, the Al component tends to dissolve more readily than the silicon components, and this allows a higher rate of condensation between silicate and aluminate species than condensation between silicate species, resulting in higher initial compressive strength [56]. In addition, the compressive strength of the alkali-activated cements also improved with the increase of Ca/Si and Ca/Al molar ratio which enhances with the incorporation of up to 75 wt% of BSS (Table 3). This is because the dissolved $Ca^{2+}$ ions can react with the Si-O-Si or Al-O-Si bonds and form C-(A)-S-H gel. Therefore, in addition to hydrated potassium aluminosilicate gel (K-A-S-H) or geopolymeric gel, hydrated calcium aluminosilicate gel (C-A-S-H) or hybrid (C,K)-A-S-H gel formation took place as indicated FTIR spectra (Fig. 9) and EDS-SEM analysis (Fig. 14) due to the amount of calcium present in the BBA but mainly in the BSS, hence the higher compressive strength of alkali activated cements containing BSS. These results are in agreement with those obtained by other authors [57–59]. These studies using steel slags and coal fly ash as precursors have shown the formation of different gels depending on the chemical and mineralogical composition of the raw materials (blast furnace slags and coal fly ash). Pastes based solely on calcium-rich slags show a predominance of C-A-S-H type gels in their structure, while in fly ash pastes rich in silicon and aluminium alkaline activated with sodium silicate, the formation of a geopolymer type N-A-S-H gel predominates. The use of both slag and fly ash precursors leads to the formation of a coexisting C-A-S-H gel and

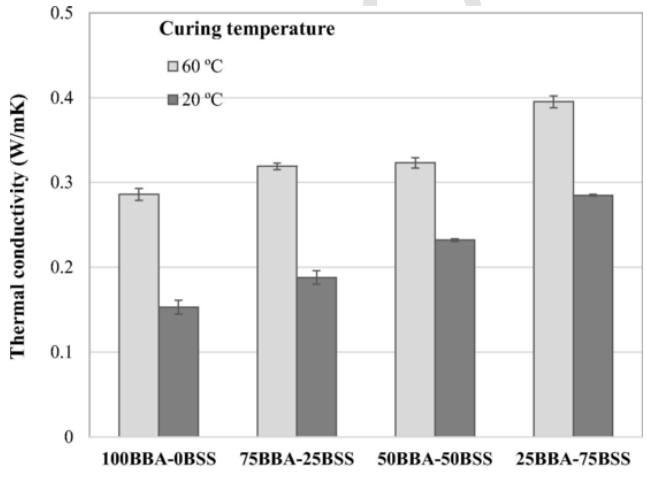


**Fig. 6.** Thermal conductivity of BBA-BSS alkali-activated pastes cured 28 days heat curing at 60 °C and 20 °C for 24 h.

geopolymer gels, which improve the mechanical properties of the materials.

Moreover, Chindraprasirt et al., [60] attributed the high calcium content in the precursors as responsible for the rapid increase in mechanical strength at early curing ages, due to their easy dissolution. The presence of Fe in BSS (25 wt%) has also been pointed out as beneficial for the development of mechanical strength of alkali-activated materials, due, like calcium, to its easy dissolution [61].

Regarding the influence of curing time, it was found that the compressive strength of specimens cured at 20 °C increased globally with increasing curing time from 1 to 90 days for all compositions. The addition of slag considerably improved the mechanical properties at low curing times, considerably increasing the compressive strength at long curing times. The optimum amount of slag to be incorporated is 50 wt%, higher additions do not produce modifications in this mechanical properties. Thus, the addition of 50 wt% produced an increase in compressive strength from 3.0 MPa of the control samples (100BBA-0BSS-20-1d) to 12.1 MPa (50BBA-50BSS-20-1d) after one day of curing increasing up to 36.6 MPa after 90 days of curing. For materials cured at 20 °C, at early ages, slightly larger pores are observed, as indicated by the SEM micrograph of sample 100BBA-0BSS-20-1d (Fig. 13 a), but smaller pores are obtained during ageing (Fig. 13 d) due to the gradual filling of the larger pores with reaction products, as the reaction progresses, which favours the increase of the compressive strength with curing time [62]. However, for the samples heat cured at 60 °C, the incorporation of BBA produced a very rapid increase in compressive strength at early ages, increasing from 10.4 MPa (control samples) to 29.9 MPa after one day of curing and increasing to 41.1 MPa for the optimum curing time, 28 days, with a decrease in compressive strength up to 35.5 MPa at 90 days of curing. Heat treatment is beneficial in increasing the reaction rate by accelerating the dissolution of silica, alumina, calcium and iron species from the silicates, facilitating the process of polycondensation and hardening of the matrix, which results in an increase in compressive strength with curing temperature. However, although the compressive strength increases with increasing curing temperature, contributing to high early strength, it may deteriorate the long-term strength at longer ages, when the degree of reaction is approximately the same, as the quality of the reaction products is the predominant parameter [62]. When heat treatment is performed, the hardening process proceeds faster, resulting in a less ordered and poorer quality structure. The higher curing temperature negatively affected the strength development at a later curing age of 90 days possibly due to modifications of the microstructure of the hydration products [63], as well as the appearance of a higher number of microcracks as indicated SEM micrographs (Fig. 13 e). Therefore, a possible reason for the decrease in compressive strength at longer curing times could be the dehydration or modification of the gel and the formation of possible micro-cracks as a result of the dehydration process for longer curing times especially when the curing environment is not saturated with water [64]. Other authors indicate an increase in mechanical properties with curing temperature up to a threshold temperature above which there is a loss of mechanical strength [32,65,66]. This threshold temperature depends on the source of aluminosilicates used and once exceeded, the time for dissolution of aluminosilicates is insufficient due to the rapid setting of the geopolymer gel formed on the surface of the undissolved particles [6,67].

The flexural strength of the alkali-activated cements as a function of curing temperature and the addition of different proportions of BSS at different curing times is shown in Fig. 5. The control sample 100BBA-0BSS cured at 20 °C did not achieve flexural strength even after 90 days of curing. At all cure times the flexural strength increased significantly with the addition of up to 50 wt% BSS and with heat curing at 60 °C at low curing times. The data reveal that the flexural strength development differs from the compressive strength data. In fact, replacing more than 50 wt% BSS caused a significant decrease in flexural strength,

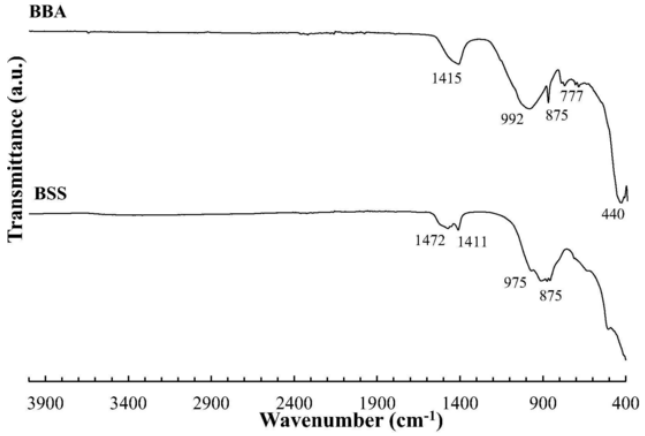


**Fig. 7.** FTIR spectra of precursor materials: BBA and BSS.

while the compressive strength remained practically unchanged. Furthermore, the flexural strength increased at all curing ages, regardless of whether the curing was thermal or room temperature, although this increase was slightly more noticeable in the 20 °C cured samples. For example, the inclusion of 50 wt% BSS increased the flexural strength from 0.90 MPa at 1 day of curing (100BAA-20-1d) to 10.88 MPa at 90 days of curing (50BBA-20-90d). Thermal curing produced an increase in flexural strength from 6.19 MPa for the control alkali-activated cements (100BBA-0BSS-60-1d) to 12.27 MPa for the alkali-activated cements 50BBA-50BSS-60-90d. The BSS have a more glassy structure as indicated by their XRD pattern. Due to their more amorphous character, BSS have a higher pozzolanic or latent-hydraulic reaction rate (Table 1) [68]. The use of BBS and thermal curing improves the flexural mechanical properties of alkali-activated cements due to the increase of bulk density and reduction of permeability [39,69]. The dissolution mechanism of the glassy phase of BSS is less dependent on the breaking of Si-O-Si and Si-O-Al bonds compared to BBA particles. This indicates faster reactions in BSS-containing mixtures compared to those containing BBA [70]. The incorporation of BSS results in the formation of more amorphous gel that fills the pores of the structure making it denser and more compact, leading to improved mechanical properties [71]. The reduction in flexural strength with the incorporation of more than 50 wt% BSS can be attributed to the development of microcracks in the alkali-activated cements as a consequence of autogenous shrinkage with cracking as indicated SEM micrographs (Fig. 14 c). The addition of BSS accelerates the reaction that causes autogenous shrinkage resulting in micro-cracks that adversely affect flexural strength [72,73].

### 3.2. Bulk density

The bulk density of the alkali-activated cements as a function of curing time and slag addition at both curing temperatures are presented in Table 4. It is evident that the bulk density increased with the addition of increasing amounts of BSS, the increase of the curing temperature from 20 to 60 °C, and with the curing age. This increase in bulk density is consistent with the trend observed for the mechanical properties. Since the real density of BSS (3245 kg/m$^3$) was higher than that of BBA (2546 kg/m$^3$), the bulk density of the geopolymer paste increased with an increase in BSS content. The increase in bulk density with thermal curing at 60 °C can be attributed to a higher dissolution of the reactive precursor phases leading to higher reaction, decreasing the number of voids in the matrix resulting in a higher amount of gel and densification of the matrix, especially at low curing times [74]. Increasing the curing

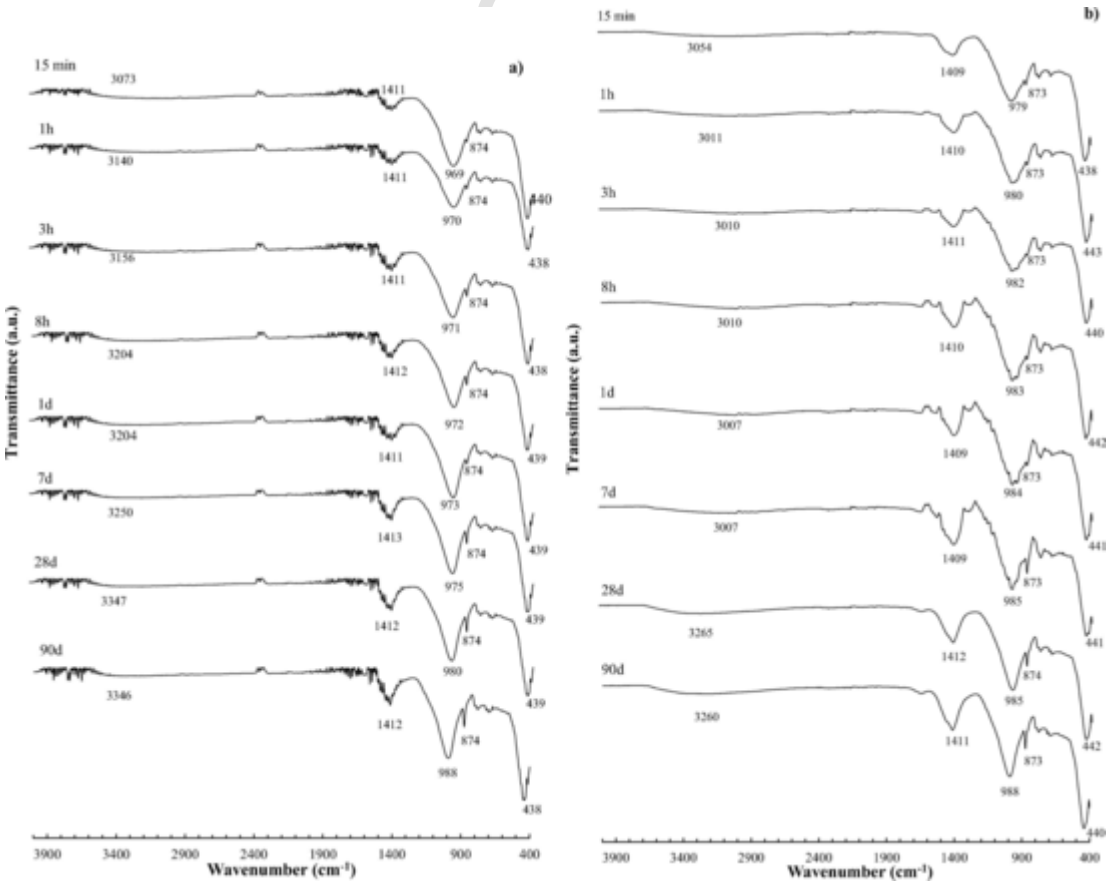


**Fig. 8.** FTIR spectra of control alkali-activated cements (100BBA-0BSS) over time for (a) heat curing at 60 °C for 24 h and (b) 20 °C..

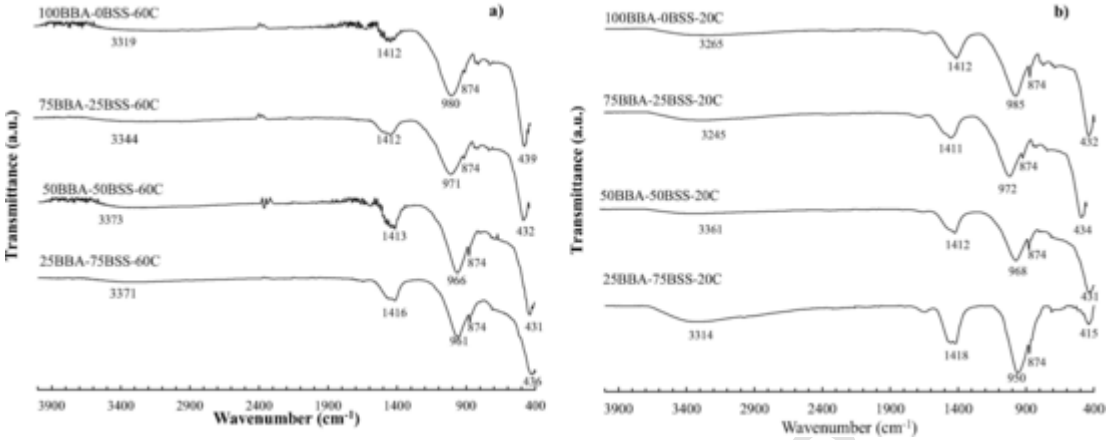


**Fig. 9.** FTIR spectra of alkali-activated cements cured at 28 days with various BSS contents (a) heat curing at 60 °C for 24 h and (b) 20 °C.

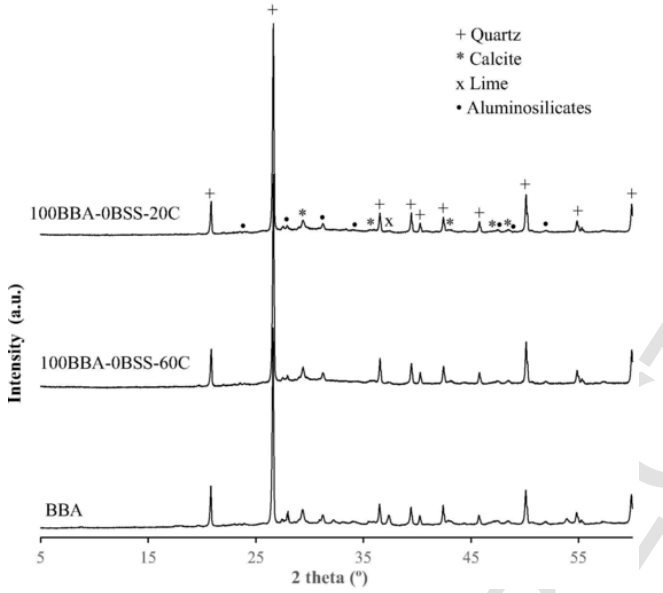


**Fig. 10.** XRD of precursor BBA and 100BBA-0BSS cured at 60 °C and 20 °C one day.

time for both curing temperatures increases the extended structure of the hydration products and reduces the porosity due to good cohesion and adhesion between the different components in the matrix leading to densification.

### 3.3. Thermal conductivity

The control alkali-activated cements after 28 days of curing exhibit thermal conductivities of 0.153 W/mK when cured at 20 °C and increased thermal conductivity to 0.286 W/mK with thermal curing at 60 °C (Fig. 6). The addition of BSS and heat curing resulted in higher thermal conductivity values, according to the bulk density data. The denser the alkali-activated cements, the higher the thermal conductivity value and the lower the thermal insulation capacity [75]. The low thermal conductivity values of the 100BBA-0BBS-20 control pastes are linked to their porous microstructure observed in SEM (Fig. 13). The presence of pores in the specimens affects the diffusion rate of heat transfer, due to the damping in the lattice vibration and the low thermal conductivity of gases in the pores much lower than that of solid substances [76,77]. The geopolymerization reaction results in amorphous and porous polysialates that restrict heat transfer. However, the higher thermal conductivity of specimens cured at 60 °C may be related to the lower porosity [78] and with the higher amount of chemically bound water providing the formation of a continuous gel for heat transfer [79].

The incorporation of BSS, which have high amounts of iron, also contributes to an increase in thermal conductivity. Therefore, the densification and distribution of the iron mineral compounds in the matrix can produce a high heat diffusion resulting in higher thermal conductivity values [32].

The specimens exhibit much lower thermal conductivity values than conventional Portland cement with conductivity values of 1.5 W/mK. [80,81]. Therefore, these less dense alkali-activated cements with high mechanical properties and high insulation capacity have advantages that make them useful for insulation purposes with structural capacity.

### 3.4. FTIR

In the precursor aluminosilicate, BBA a band centred at 993 $cm^{-1}$ attributed to the bending vibration of the Si-O-T bond (T = Si or Al) and a band centred at 440 $cm^{-1}$ attributed to the bending vibration of the Si-O bond are observed (Fig. 7) [82,83].

After activation of the precursor with the alkaline solution the asymmetric stretching vibration of the Si-O-T bonds (T = Si or Al) after 15 min shifted to lower frequencies 979 $cm^{-1}$ and 969 $cm^{-1}$ in spectra 100BBA-0BSS-20 and 100BBA-0BSS-60, suggesting the development of a new K-A-S-H gel product, being the footprint of the geopolymerization process (Fig. 8) [84], as well as, the formation of a calcium silicate (C-(A)-S-H) type gel [85,86]. This shift and intensity of the band was more pronounced in pastes heat cured at 60 °C. This indicates that increasing the temperature from 20 to 60 °C favours the dissolution of the BBA in the alkaline solution by increasing the amount of binder within the matrix, especially at low cure times. The higher intensity of the band with curing time indicates the development of a higher amount of gel at older ages. Therefore, this result confirms that the curing temperature of 60 °C accelerates the geopolymerization process [87]. The shift towards higher frequencies observed in that band, as the reaction time increases, indicates a higher degree of polymerization [86]. Both facts justify an increase to better mechanical properties of the alkali-activated control cements with curing time, and the improvement of mechanical properties in specimens cured at 60 °C, especially at low curing times.

The spectra of the alkali-activated cements cured at 60 °C or at 20 °C incorporating BSS after 28 days of curing are presented in Fig. 9. It can be observed in the spectra of the heat cured pastes and those cured at room temperature a shift of the band characteristic of the geopolymerization process from approximately 980 $cm^{-1}$ for the 100BBA-0BSS to 961 $cm^{-1}$ for the 25BBA-75BSS. The incorporation of BSS, due to its more amorphous character, as well as, the curing temperature produced a higher dissolution in the alkaline solution leading to the forma-

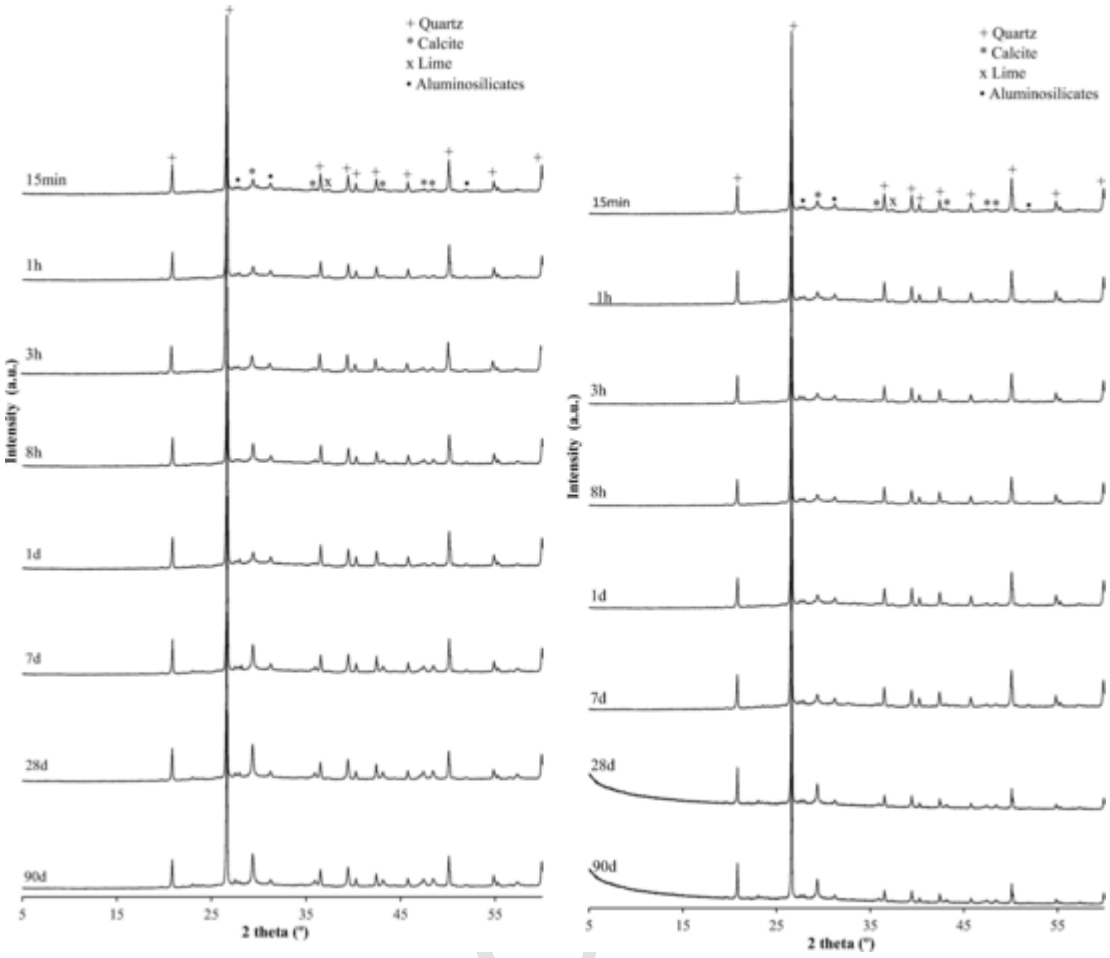


**Fig. 11.** XRD of control alkali-activated cements (100BBA-0BSS) over time for (a) heat curing at 60 °C for 24 h and (b) 20 °C.

tion of a higher amount of geopolymer gel and C-(A)-S-H gel [86]. In addition, this displacement could be associated with the introduction of Ca and Fe ions in the -Si-O- bond confirming the existence of Ca(K)-(A)-S-H gel [88,89]. The increase in the amount of gel formed with the addition of BSS justifies an increase in the flexural and compressive strength of the specimens.The absorption bands centred at approximately 3350 $cm^{-1}$ and 1650 $cm^{-1}$ are linked to the bending of the H-O–H bond and the O–H bond of water molecules [90,91]. This band corresponds to water molecules from the crystallisation or absorption of reaction products [92]. These bands do not appear in the precursors (BBA and BSS) and show the geopolymerization reaction of alkaline activation products and water in the paste. This band is slightly smaller as the curing time increases, and in the alkali-activated cements heat cured at 60 °C, which could be due to a higher water consumption during the alkaline activation reaction. The bands in the samples centred at 1412 and 874 $cm^{-1}$ indicated the presence of the $CO_3^{2-}$ group formed from the reaction between unreacted potassium ions that leach out of the matrix and react with atmospheric $CO_2$ producing the carbonation of the alkali-activated material [22,91].

The band centered at 874 $cm^{-1}$ can be assigned to the symmetric vibrational deformation of the C-O-C bond in 100BBA-0BSS, while in slag-containing alkali-activated cements it can also be assigned to the vibrational mode of the Si-O-Fe bond [93].

### 3.5. XRD analysis

Fig. 10 shows the X-ray diffraction patterns of the control sample 100BBA-0BSS after 1 day of curing at 60 °C and 20 °C. As a comparison, the XRD pattern of the BBA raw material is shown. In both series already after 15 min a pronounced amorphous halo in the 2 theta range between 20 and 40 ° was observed, which justifies the effective formation of the geopolymer binder obtained by the dissolution of the reactive phase contained in the solid precursor, BBA. However, after alkaline activation the crystalline mineralogical phases present in the precursor such as quartz ($SiO_2$) and calcite ($CaCO_3$) remain almost unchanged in the alkali-activated pastes. The quartz phase is largely non-reactive [92]. Furthermore, the intensity of most of the diffraction peaks did not differ substantially in alkali-activated cements cured at different temperatures (60 and 20 °C), although the intensity of diffraction peaks associated with quartz and aluminosilicates is slightly lower for 100BBA-0BSS specimens cured at 60 °C. Moderate heat curing at 60 °C produced a higher surface attack of the crystalline phases providing reactive silica and promoting the formation of gel, increasing the compressive strength at early ages. Although the high intensity of the quartz peak in the specimens indicated that quartz practically did not participate in the alkaline activated reaction [94]. Therefore, as reported by other studies [95], the curing temperature has hardly any influence on the transformation of the crystalline phases present in the precursor and the structural changes occur in the amorphous phase. Tian et al., 2020 [96] reported that the intensity of the peaks attributed to illite ($KAl_2[(SiAl)_4O_{10}](OH)_2nH_2O$) and quartz ($SiO_2$) present in the precursor the copper tailings decreased as the curing temperature increases from 20 to 80 °C and increased as the curing temperature increased from 100 and 120 °C. Yao et al. [97] reported that under the strong alkaline activation conditions, the metakaolin muscovite underwent the geopolymerization process, which increased as the curing temperature increased from 20 to 80 °C, while the quartz phase remained largely unreactive.

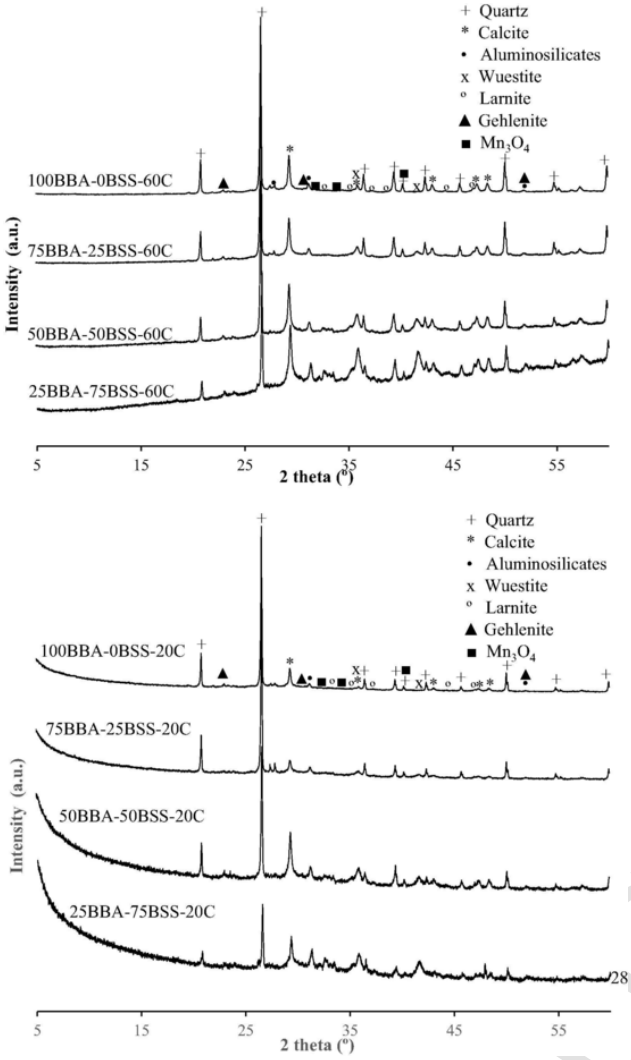


**Fig. 12.** XRD of alkali-activated cements cured at 28 days with various BSS contents (a) heat curing at 60 °C for 24 h and (b) 20 °C.

Regarding the influence of the curing time, it can be observed that there are practically no differences in the diffractograms of the alkali-activated cements with curing time, at both curing temperatures (Fig. 11). These crystalline phases are not reactive, there is no dissolution of the crystalline phases with time and therefore they are present as inert fillers in the alkali-activated binder. Therefore, only the amorphous phases in the raw materials are reactive and contribute to alkaline activated reaction [97–100]. Only a slight increase of the diffraction peak corresponding to $CaCO_3$ was observed as the curing time increases, due to unreacted excess KOH rising to the surface and reacting with atmospheric $CO_2$ to form carbonates, as evidenced by FTIR.

The diffractograms of the alkali-activated cements incorporating BSS at both curing temperatures after 28 days of curing (Fig. 12) show the diffraction peaks appearing in the BBA precursor. The intensity of cristaline peaks decreasing as additional amounts of BSS are incorporated due to the relatively amorphous character of the residue. Only a higher intensity of diffraction peaks associated with undissolved ingredients present in the BSS as wustite is observed. These results indicate that specimens incorporating BSS have a higher amount of amorphous as indicated by the higher deviation from the baseline at 2 theta between 25 and 35° although difractograms also include crystalline phases as impurities and inclusions. The increased amount of amorphous phases in the BSS, led to an increase in the mechanical properties of the alkali-activate cements incorporating the residue.

### 3.6. Microstructural analysis

SEM images showed that the alkali-activated control materials 100BBA-0BBS (Fig. 13) after one day of curing present a compact and dense structure, although with the presence of fine cracks, more visible in the heat-cured specimens. Partially reacted BBA particles, dense gel phase and a fibrous structure corresponding to the K-(A)-S-H gel were observed. The presence of two types of gel, K-(A)-S-H and C-(A)-S-H has been confirmed by SEM-EDS analysis. The EDS spectra of spot 1 showed intense peaks of Si, Al and K, suggesting the production of potassium aluminosilicate gel (K-A-S-H) or geopolymeric gel, while the EDS spectra of spot 2 show intense peaks of Si, Al and Ca, indicating the formation of calcium aluminosilicate gel (C-A-S-H). Less intense peaks of Ca (point 1) and K (point 2) were observed in both areas, which may suggest the formation of a hydrated calcium potassium calcium aluminosilicate gel (K-C-A-S-H) in both areas.

In the control pastes cured at 20 °C, a more heterogeneous matrix was observed with less gel phase extension, higher porosity and more unreacted BBA particles, which could still participate in the alkaline activated reaction at longer curing times (Fig. 14). This suggests that a moderately high curing temperature of 60 °C promotes the dissolution of aluminosilicates and calcium phases from the precursor and the formation of new polymer chains, resulting in a higher amount of geopolymer gel and C-(A)-S-H gel and improved compressive strength at early curing ages according with mechanical strength data. As for the influence of curing time, a higher amount of geopolymer gel and C-(A)-S-H gel and a lower amount of unreacted BBA particles were observed as the curing time increases from 1 to 28 days, with the microstructure remaining almost constant at longer curing times (90 days). Control alkali-activated cements cured at 20 °C present lower porosity and a denser structure when the curing time increases from 1 to 28 days. The pozzolanic activity of BBA increases over an extended period. Porosity in pastes is associated with gel formation and also with the presence of water in capillaries that are not filled by the alkaline activated reaction. The more the material reacts, the more geopolymer chains are formed and the number of pores is reduced, indicating the progress of the geopolymerization reaction with the curing time [101]. As the reactions progress, by the age of 28 days of curing, most of the BBA particles have reacted to form dense amorphous products which resulted in an increase in compressive strength.

The incorporation of BSS resulted in a higher densification with a less porous structure compared to the control samples (Fig. 14). Gel formation was observed over the entire fracture surface. In general, BBS contains a higher proportion of calcium, which favours the formation of calcium aluminosilicate (C-A-S-H) gel [57,58]. The gel phase compositions determined by EDS analysis, indicate higher Ca intensity which could indicate the active participation of Ca to produce more calcium rich Ca-(K)-A-S-H hydrated aluminosilicate gel in the BBA-BSS blended alkali-activated cements which produced denser microstructure and higher compressive strength compared to the control 100 % BBA pastes according to flexural and compression strength data. In the 50BBA-50BSS-60-28d alkali-activated cements, iron-rich zones are also observed in some regions, which could indicate the dissolution of the metal and its participation in the gel phase.

Heat cured samples incorporating BSS showed a higher number of micro-cracks. These cracks are mainly due to autogenous shrinkage of the specimen due to heat and slag incorporation. The amount of cracks is not very high because the specimens were cured at high relative humidity. These results confirm the low flexural strength values obtained for the 25BBA-75BSS-60 specimens, which have a more heterogeneous structure and a higher number of micro-cracks.

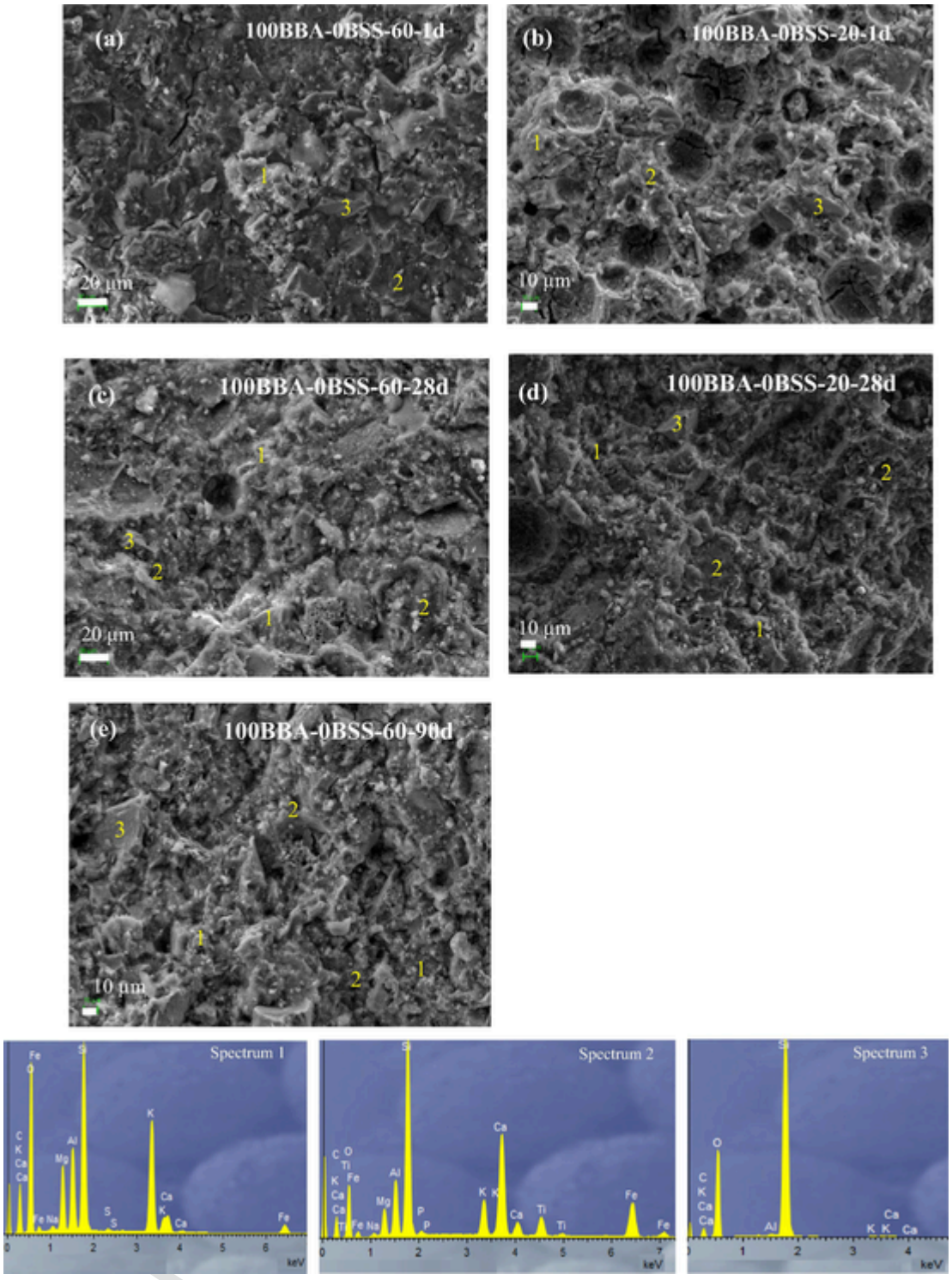


**Fig. 13.** SEM-EDS of control alkali-activated cements (100BBA-0BSS) over time heat curing at 60 °C and 20 °C for 24 h.(a) 100BBA-0BSS-60-1d; (b) 100BBA-0BSS-60-1d; (c) 100BBA-0BSS-60-28d; (d)100BBA-0BSS-20-1d; (e) 100BBA-0BSS-60-90d.

## 4. Conclusions

In this work, the effect of the incorporation of different amounts of BSS to alkali-activated BBA-based cements and the effect of the curing temperature 60 °C and 20 °C have been investigated. The following conclusions can be drawn:

- Heat curing at 60 °C produced an increase in mechanical properties, mainly at early curing ages, probably due to an increased dissolution of reactive species. However, similar or better mechanical properties are obtained for specimens cured at 20 °C at longer curing times. The addition of BSS also has a good effect on the mechanical properties.
- The compressive strength of the alkali-activated cements increased with decreasing Si/Al molar ratio because the silicate gel does not contribute significantly to the mechanical strength, the aluminosilicate gel being stronger. The high CaO content in the BSS may help to form a higher amount of C-A-S-H gel together with the K-A-S-H gel, or the formation of a hybrid (C,K)-A-S-H gel being

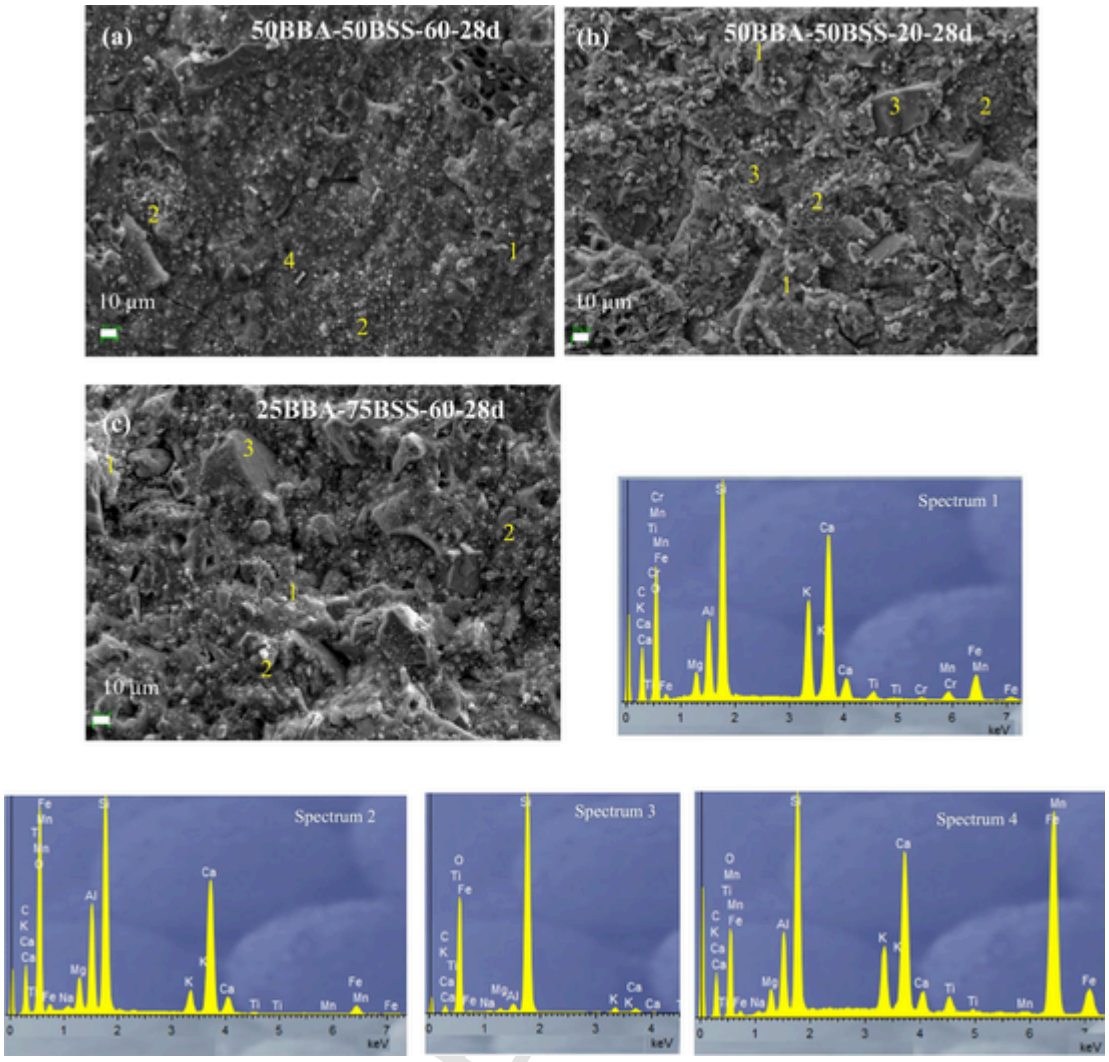


**Fig. 14.** SEM-EDS of (a) 50BBA-50BSS pastes cured 28 days heat curing at 60 °C for 24 h and (b) 50BBA-50BSS pastes cured 28 days heat curing at 20 °C and (c) 75BBA-25BBS pastes cured 28 dias heat curing at 60 °C for 24 h.

responsible for the rapid increase of mechanical strengths at early curing ages.

- Higher compressive strength and flexural strength of the alkali-activated pastes was obtained with increasing incorporation of up to 50 wt% slag. The compressive strength increases overall with increasing curing time from 1 to 28 days for all compositions cured at 60 °C, up to an optimum value of 41.1 MPa. Curing times longer than 90 days produced a decrease in compressive strength, possibly due to the lower quality of the reaction products, more dehydration of the gel and the formation of possible micro-cracks and carbonation over a prolonged period, which led to deteriorations of the mechanical properties. For room temperature cured pastes, a more pronounced increase is observed with curing time from 1 to 90 days, reaching similar or even higher values at longer curing times than the heat cured specimens, with compressive strength values of 36.6 MPa.
- At all curing times the flexural strength increased with the addition of up to 50 wt% BSS and with heat curing at 60 °C. The addition of BSS results in the formation of more amorphous gel making the structure more dense and compact, which leads to an improvement of the mechanical properties. The addition of 75 wt% BSS greatly accelerated the alkaline activated reaction causing rapid autogenous shrinkage resulting in micro-cracks which negatively affect the flexural strength.
- The thermal conductivity of the pastes increased with the incorporation of BSS and with the curing temperature from 20 °C to 60 °C. This increase could be related to the densification of the samples and the distribution of iron minerals in the matrix present in the BSS waste. However, all alkali-activated cements show thermal conductivities lower than 0.4 W/mK, presenting higher thermal insulation capacity than the Portland cement binder with thermal conductivities of 1.5 W/mK.

Therefore, the results indicate that the valorisation of BBA (a waste from pine and olive pruning combustion) with the incorporation of BSS (a waste from iron and steel production) is possible to obtain alkali-activated cements cured at room temperature with technological properties suitable to replace Portland cement binders. The development of these new construction materials with structural properties has important socio-economic and environmental benefits by converting waste into by-products and avoiding landfill. In addition, their manufacture reduces $CO_2$ emissions into the atmosphere and the depletion of mineral resources compared to Portland cement binders.

## CRediT authorship contribution statement

**M.A. Gómez-Casero:** Investigation, Data curation, Writing – original draft, Writing – review & editing. **L. Pérez-Villarejo:** Conceptual-

ization, Methodology, Validation, Formal analysis, Writing – review & editing. **E. Castro:** Writing – review & editing. **D. Eliche-Quesada:** Conceptualization, Formal analysis, Investigation, Data curation, Resources, Supervision, Project administration, Funding acquisition, Visualization, Writing – original draft, Writing – review & editing.

## Declaration of Competing Interest

The authors declare that they have no known competing financial interests or personal relationships that could have appeared to influence the work reported in this paper.

## Acknowledgements

This work has been funded by the project Development and characterization of new geopolymeric composites based on waste from the olive industry. Towards a sustainable construction (MAT2017-88097-R), FEDER / Ministry of Science, Innovation and Universities, State Research Agency. The authors thank "Aldebarán Energía del Guadalquivir S.L." company and "Siderúrgica Sevillana S.A." for supplying the biomass bottom ash and black steel slag, respectively. M.A. Gómez-Casero acknowledges support of MINECO (PRE2018-084073). Technical and human support provided by CICT of Universidad de Jaén (UJA, MINECO, Junta de Andalucía, FEDER) is gratefully acknowledged.

## References

[1] J.L. Provis, Alkali-activated materials, Cem Concr Res. 114 (2018) 40–48, https://doi.org/10.1016/j.cemconres.2017.02.009.
[2] A. Palomo, M.W. Grutzeck, M.T. Blanco, Alkali-activated fly ashes: a cement for the future, Cem. Concr. Res. 29 (8) (1999) 1323–1329, https://doi.org/10.1016/S0008-8846(98)00243-9.
[3] Properties of Geopolymer Cements 1 (1994) 131–149.
[4] J. Davidovits, Geopolymers and geopolymeric materials, J. Therm. Anal. 35 (2) (1989) 429–441, https://doi.org/10.1007/BF01904446.
[5] F. Pacheco-Torgal, Z. Abdollahnejad, A.F. Camões, M. Jamshidi, Y. Ding, Durability of alkali-activated binders: a clear advantage over Portland cement or an unproven issue?, Constr. Build. Mater. 30 (2012) 400–405, https://doi.org/10.1016/j.conbuildmat.2011.12.017.
[6] J. Davidovits, Geopolymer chemistry and applications, Saint Quentin, Geopolymer Institute, 2008.
[7] F.G.M. Aredes, T.M.B. Campos, J.P.B. Machado, K.K. Sakane, G.P. Thim, D.D. Brunelli, Effect of cure temperature on the formation of metakaolinite-based geopolymer, Ceram. Int. 41 (6) (2015) 7302–7311, https://doi.org/10.1016/j.ceramint.2015.02.022.
[8] O. Ayeni, A.P. Onwualu, E. Boakye, Characterization and mechanical performance of metakaolin-based geopolymer for sustainable building applications, Constr. Build. Mater. 272 (2021) 121938, https://doi.org/10.1016/j.conbuildmat.2020.121938.
[9] N. Essaidi, B. Samet, S. Baklouti, S. Rossignol, Feasibility of producing geopolymers from two different Tunisian clays before and after calcination at various temperatures, Appl. Clay Sci. 88 (2014) 221–227, https://doi.org/10.1016/j.clay.2013.12.006.
[10] S. Andrejkovičová, A. Sudagar, J. Rocha, C. Patinha, W. Hajjaji, E.F. da Silva, A. Velosa, F. Rocha, The effect of natural zeolite on microstructure, mechanical and heavy metals adsorption properties of metakaolin based geopolymers, Appl. Clay Sci. 126 (2016) 141–152, https://doi.org/10.1016/j.clay.2016.03.009.
[11] M. Amran, S. Debbarma, T. Ozbakkaloglu, Fly ash-based eco-friendly geopolymer concrete: A critical review of the long-term durability properties, Constr. Build. Mater. 270 (2021) 121857, https://doi.org/10.1016/j.conbuildmat.2020.121857.
[12] W.K.W. Lee, J.S.J. Van Deventer, The effect of ionic contaminants on the early-age properties of alkali-activated fly ash-based cements, Cem. Concr. Res. 32 (2002) 577–584, https://doi.org/10.1016/S0008-8846(01)00724-4.
[13] A.M. Rashad, A comprehensive overview about the influence of different admixtures and additives on the properties of alkali-activated fly ash, Mater. Des 53 (2014) 1005–1025, https://doi.org/10.1016/j.matdes.2013.07.074.
[14] I.H. Aziz, M.M. Al Bakri-Abdullah, M.A.A. Mohd-Salleh, E. Aizat-Azimi, J. Chaiprap, A.V. Sandu, Strength development of solely ground granulated blast furnace slag geopolymers, Constr. Build. Mater. 250 (2020) 118720. 10.1016/j.conbuildmat.2020.118720
[15] A. Gupta, Investigation of the strength of ground granulated blast furnace slag based geopolymer composite with silica fume, Mater. Today-Proc. In Press (2020), https://doi.org/10.1016/j.matpr.2020.06.010.
[16] S. Shagñay, F. Velasco, A. del Campo, M. Torres-Carrasco, Wear behavior in pastes of alkali-activated materials: Influence of precursor and alkali solution, Tribol. Int. 147 (2020) 106293, https://doi.org/10.1016/j.triboint.2020.106293.
[17] F. Puertas, Cementos de escorias activadas alcalinamente: Situación actual y perspectivas de futuro, Mater. Construcc. 45 (239) (1995) 53–64, https://doi.org/10.3989/mc.1995.v45.i23910.3989/mc.1995.v45.i239.553.
[18] H. Xu, J.S.J. Van Deventer, Geopolymerisation of multiple minerals, Miner. Eng. 15 (12) (2002) 1131–1139, https://doi.org/10.1016/S0892-6875(02)00255-8.
[19] T.W. Cheng, J.P. Chiu, Fire-resistant geopolymer produced by granulated blast furnace slag, Miner. Eng. 16 (2003) 205–210, https://doi.org/10.1016/S0892-6875(03)00008-6.
[20] A. Autef, E. Joussein, G. Gasgnier, S. Rossignol, Role of the silica source on the geopolymerization rate: a thermal analysis study, J. Non-Cryst. Solids 366 (2013) 13–21, https://doi.org/10.1016/j.jnoncrysol.2013.01.034.
[21] M.B. Karakoc, I. Türkmen, M.M. Maraş, F. Kantarci, R. Demirboğa, Sulfate resistance of ferrochrome slag based geopolymer concrete, Ceram. Int. 42 (2016) 1254–1260, https://doi.org/10.1016/j.ceramint.2015.09.058.
[22] M. Torres-Carrasco, F. Puertas, Waste glass in the geopolymer preparation. Mechanical and microstructural characterisation, J. Clean. Prod. 90 (2015) 397–408, https://doi.org/10.1016/j.jclepro.2014.11.074.
[23] E. Papa, V. Medri, E. Landi, B. Ballarin, F. Miccio, Production and characterization of geopolymers based on mixed compositions of metakaolin and coal ashes, Mater. Des. 56 (2014) 409–415, https://doi.org/10.1016/j.matdes.2013.11.054.
[24] A. Peys, H. Rahier, Y. Pontikes, Potassium-rich biomass ashes as activators in metakaolin-based inorganic polymers, Appl. Clay Sci. 119 (2016) 401–409, https://doi.org/10.1016/j.clay.2015.11.003.
[25] M.J.B. Moraes, J.C.B. Moraes, M.M. Tashima, J.L. Akasaki, L. Soriano, M.V. Borrachero, J. Payá, Production of bamboo leaf ash by auto-combustion for pozzolanic and sustainable use in cementitious matrices, Constr. Build. Mater. 208 (2019) 369–380, https://doi.org/10.1016/j.conbuildmat.2019.03.007.
[26] R.S. Padhi, R.K. Patra, B.B. Mukharjee, T. Dey, Influence of incorporation of rice husk ash and coarse recycled concrete aggregates on properties of concrete, Constr. Build. Mater. 173 (2018) 289–297, https://doi.org/10.1016/j.conbuildmat.2018.03.270.
[27] S.V. Vassilev, D. Baxter, L.K. Andersen, C.G. Vassileva, An overview of the composition and application of biomass ash. Part 1. Phase–mineral and chemical composition and classification, Fuel 105 (2013) 40–76, https://doi.org/10.1016/j.fuel.2012.09.041.
[28] A. Fernandez-Jimenez, A. Palomo, Characterisation of fly ashes potential reactivity as alkaline cements, Fuel 82 (2003) 2259–2265, https://doi.org/10.1016/S0016-2361(03)00194-7.
[29] R.A.A.B. Santa, C. Soares, H.G. Riella, Geopolymers obtained from bottom ash as source of aluminosilicate cured at room temperature, Constr. Build. Mater. 157 (2017) 459–466, https://doi.org/10.1016/j.conbuildmat.2017.09.111.
[30] A. Sathonsaowaphak, P. Chindaprasirt, K. Pimraksa, Workability and strength of lignite bottom ash geopolymer mortar, J. Hazard. Mater. 168 (1) (2009) 44–50, https://doi.org/10.1016/j.jhazmat.2009.01.120.
[31] P. Chindaprasirt, C. Jaturapitakkul, W. Chalee, U. Rattanasak, Comparative study on the characteristics of fly ash and bottom ash geopolymers, Waste Manag. 29 (2) (2009) 539–543, https://doi.org/10.1016/j.wasman.2008.06.023.
[32] C. Rodrigue Kaze, P. Ninla Lemougna, T. Alomayri, H. Assaedi, A. Adesina, S. Kumar Das, G.-L. Lecomte-Nana, E. Kamseu, U. Chinje Melo, C. Leonelli, Characterization and performance evaluation of laterite based geopolymer binder cured at different temperatures, Constr. Build. Mater. 270 (2021) 121443, https://doi.org/10.1016/j.conbuildmat.2020.121443.
[33] M. Zribi, B. Samet, S. Baklouti, Effect of curing temperature on the synthesis, structure and mechanical properties of phosphate-based geopolymers, J. Non-Cryst. Solids 511 (2019) 62–67, https://doi.org/10.1016/j.jnoncrysol.2019.01.032.
[34] Y. Zhang, R. Xiao, X. Jiang, W. Li, X. Zhu, B. Huang, Effect of particle size and curing temperature on mechanical and microstructural properties of waste glass-slag-based and waste glass-fly ash-based geopolymers, J. Clean. Prod. 273 (2020) 122970, https://doi.org/10.1016/j.jclepro.2020.122970.
[35] X. Tian, W. Xu, S. Song, F. Rao, L. Xia, Effects of curing temperature on the compressive strength and microstructure of copper tailing-based geopolymers, Chemosphere 253 (2020) 126754, https://doi.org/10.1016/j.jclepro.2020.122970.
[36] M.S.H. Khan, A. Castel, A. Akbarnezhad, S.J. Foster, M. Smith, Utilisation of steel furnace slag coarse aggregate in a low calcium fly ash geopolymer concrete, Cem. Concr. Res. 89 (2016) 220–229, https://doi.org/10.1016/j.cemconres.2016.09.001.
[37] W. Song, Z. Zhu, Y. Peng, Y.u. Wan, X. Xu, S. Pu, S. Song, Y. Wei, Effect of steel slag on fresh, hardened and microstructural properties of high-calcium fly ash based geopolymers at standard curing condition, Constr. Build. Mater. 229 (2019) 116933, https://doi.org/10.1016/j.conbuildmat.2019.116933.
[38] P. Zhang, Z. Gao, J. Wang, J. Guo, S. Hu, Y. Ling, Properties of fresh and hardened fly ash/slag based geopolymer concrete: A review, J. Clean. Prod. 270 (2020) 122389, https://doi.org/10.1016/j.jclepro.2020.122389.
[39] M.A. Yazdi, M. Liebscher, S. Hempel, J. Yang, V. Mechtcherine, Correlation of microstructural and mechanical properties of geopolymers produced from fly ash and slag at room temperature, Constr. Build. Mater. 191 (2018) 330–341, https://doi.org/10.1016/j.conbuildmat.2018.10.037.
[40] S. Saha, C. Rajasekaran, Enhancement of the properties of fly ash based geopolymer paste by incorporating ground granulated blast furnace slag, Constr. Build. Mater. 146 (2017) 615–620, https://doi.org/10.1016/j.conbuildmat.2017.04.139.
[41] C.B. Cheah, M.H. Samsudin, M. Ramli, W.K. Part, L.E. Tan, The use of high calcium wood ash in the preparation of Ground Granulated Blast Furnace Slag and Pulverized Fly Ash geopolymers: A complete microstructural and mechanical characterization, J. Clean. Prod. 156 (2017) 114–123, https://doi.org/10.1016/j.jclepro.2017.04.026.

[42] S.K. Nath, S. Kumar, Influence of iron making slags on strength and microstructure of fly ash geopolymer, Constr. Build. Mater. 38 (2013) 924–930, https://doi.org/10.1016/j.conbuildmat.2012.09.070.
[43] E. Bonet-Martínez, P. García-Cobo, L. Pérez-Villarejo, E. Castro, D. Eliche-Quesada, Effect of Olive-Pine Bottom Ash on Properties of Geopolymers Based on Metakaolin, Materials 13 (2020) 13, 901. 10.3390/ma13040901.
[44] T. Xie, P. Visintin, A unified approach for mix design of concrete containing supplementary cementitious materials based on reactivity moduli, J. Clean. Prod. 203 (2018) 68–82, https://doi.org/10.1016/j.jclepro.2018.08.254.
[45] A. Karrech, M. Dong, M. Elchalakani, M.A. Shahin, Sustainable geopolymer using lithium concentrate residues, Construct. Build. Mater. 228 (2019) 116740, https://doi.org/10.1016/j.conbuildmat.2019.116740.
[46] S.F.A.S. Shah, B. Chen, M.R. Ahmad, M.A. Haque, Development of Cleaner One-part geopolymer from lithium slag, J. Clean. Prod. 291 (2021) 1125241, https://doi.org/10.1016/j.jclepro.2020.125241.
[47] T. Luukkonen, Z. Abdollahnejad, J. Yliniemi, P. Kinnunen, M. Illikainen, Onepart alkali-activated materials: a review, Cem. Concr. Res. 103 (2018) 21–34, https://doi.org/10.1016/j.cemconres.2017.10.001.
[48] A.M. Rashad, An investigation of high-volume fly ash concrete blended with slag subjected to elevated temperatures, J. Clean. Prod. 93 (2015) 47–55, https://doi.org/10.1016/j.jclepro.2015.01.031.
[49] UNE-EN 1015-10:2000. Methods of test for mortar for masonry - Part 10: Determination of dry bulk density of hardened mortar.
[50] UNE-EN 1015-11:2000/A1:2007. Methods of test for mortar for masonry - Part 11: Determination of flexural and compressive strength of hardened mortar.
[51] ISO-8302,1991. Thermal insulation - Determination of steady-state thermal resistance and related properties - Guarded hot plate apparatus.
[52] A. Fernández-Jiménez, A.G. de la Torre, A. Palomo, G. López-Olmo, M.M. Alonso, M.A.G. Aranda, Quantitative determination of phases in the alkaline activation of fly ash, Part II: Degree of reaction, Fuel. 85 (14–15) (2006) 1960–1969, https://doi.org/10.1016/j.fuel.2006.04.006.
[53] P. Nath, P.K. Sarker, Use of OPC to improve setting and early strength properties of low calcium fly ash geopolymer concrete cured at room temperature, Cem. Concr. Comp. 55 (2015) 205–214, https://doi.org/10.1016/j.cemconcomp.2014.08.008.
[54] J.S.J. van Deventer, R. San Nicolas, I. Ismail, S.A. Bernal, D.G. Brice, J.L. Provis, Microstructure and durability of alkali-activated materials as key parameters for standardization, J. Sustain. Cem. Based Mater. 4 (2) (2015) 116–128, https://doi.org/10.1080/21650373.2014.979265.
[55] A. Fernández-Jiménez, A. Palomo, I. Sobrados, J. Sanz, The role played by the reactive alumina content in the alkaline activation of fly ashes, Micr. Mesop. Mater. 91 (1–3) (2006) 111–119, https://doi.org/10.1016/j.micromeso.2005.11.015.
[56] N. Ranjbar, M. Mehrali, U.J. Alengaram, H.S.C. Metselaar, M.Z. Jumaat, Compressive strength and microstructural analysis of fly ash/palm oil fuel ash based geopolymer mortar under elevated temperatures, Const. Build. Mater. 65 (2014) 114–121, https://doi.org/10.1016/j.conbuildmat.2014.04.064.
[57] I. Ismail, S.A. Bernal, J.L. Provis, R. San Nicolas, S. Hamdan, J.S.K. van Deventer, Modification of phase evolution in alkali-activated blast furnace slag by the incorporation of fly ash, Cem. Concr. Comp. 45 (2014) 125-135. https://doi.org/10.1016/j.cemconcomp.2013.09.006
[58] A. Bouaissi, L. Li, M.M.A.B. Abdullah, Q. Bui, Mechanical properties and microstructure analysis of FA-GGBS-HMNS based geopolymer concrete, Constr. Build. Mater. 210 (2019) 198–209, https://doi.org/10.1016/j.conbuildmat.2019.03.202.
[59] P. Nath, P.K. Sarker, Effect of GGBFS on setting, workability and early strength properties of fly ash geopolymer concrete cured in ambient condition, Constr. Build. Mater. 66 (2014) 163-71. 10.1016/j.conbuildmat.2014.05.080
[60] P. Chindaprasirt, T. Chareerat, S. Hatanaka, T. Cao, High-strength geopolymer using fine high-calcium fly ash, J. Mater. Civil Eng. 23 (3) (2011) 264–270, https://doi.org/10.1061/(ASCE)MT.1943-5533.0000161.
[61] E. Adesanya, K. Ohenoja, A. Di Maria, P. Kinnunen, M. Illikainen, Alternative alkali-activator from Steel-making Waste for one-part alkali-activated slag, J. Clean. Prod. 274 (2020) 123020, https://doi.org/10.1016/j.jclepro.2020.123020.
[62] P. Rovnaník, Effect of curing temperature on the development of hard structure of metakaolin-based geopolymer, Constr. Build. Mater. 24 (7) (2010) 1176–1183, https://doi.org/10.1016/j.conbuildmat.2009.12.023.
[63] Y. Maltais, J. Marchand, Influence of curing temperature on cement hydration and mechanical strength development of fly ash mortars, Cem. Concr. Res. 27 (7) (1997) 1009–1020, https://doi.org/10.1016/S0008-8846(97)00098-7.
[64] Y.M. Liew, C.Y. Heah, A.B. Mohd Mustafa, H. Kamarudin, Structure and properties of clay-based geopolymer cements: a review, Prog. Mater. Sci. 83 (2016) 595–629, https://doi.org/10.1016/j.pmatsci.2016.08.002.
[65] P.N. Lemougna, K. Wang, Q. Tang, U.C. Melo, X. Cui, Recent developments on inorganic polymers synthesis and applications, Ceram. Int. 42 (2016) 15142–15159, https://doi.org/10.1016/j.ceramint.2016.07.027.
[66] T. Suwan, M. Fan, N. Braimah, Micro-mechanisms and compressive strength of Geopolymer-Portland cementitious system under various curing temperatures, Mater. Chem. Phys. 180 (2016) 219–225, https://doi.org/10.1016/j.matchemphys.2016.05.069.
[67] P.N. Lemougna, K. Wang, Q. Tang, X. Cui, Study on the development of inorganic polymers from red mud and slag system: application in mortar and lightweight materials, Constr. Build. Mater. 156 (2017) 486–495, https://doi.org/10.1016/j.conbuildmat.2017.09.01.
[68] C. Li, H. Sun, L. Li, A review: the comparison between alkaliactivated slag (Si + Ca) and metakaolin (Si + Al) cements, Cem. Concr. Res. 40 (2010) 1341–1349, https://doi.org/10.1016/j.cemconres.2010.03.020.
[69] I. Ismail, S.A. Bernal, J.L. Provis, R.S. Nicolas, G. David, A.R. Brice, S. Kilcullen, J. S.J. Hamdan, van Deventer, Influence of fly ash on the water and chloride permeability of alkali-activated slag mortars and concretes, Constr. Build. Mater. 48 (2013) 1187–1201, https://doi.org/10.1016/j.conbuildmat.2013.07.106.
[70] C. Galle, Effect of drying on cement-based materials pore structure as identified by mercury intrusion porosimetry: a comparative study between oven-, vacuum-, and freeze-drying, Cem. Concr. Res. 31 (2001) 1467–1477, https://doi.org/10.1016/S0008-8846(01)00594-4.
[71] A. Aziz, O. Stocker, I.E. El Hassani, A.P. Laborier, E. Jacotot, A. El Khadiri, A. El Bouari, Effect of blast-furnace slag on physicochemical properties of pozzolan-based geopolymers, Mater. Chem. Physics 258 (2021) 123880, https://doi.org/10.1016/j.matchemphys.2020.123880.
[72] N. Ismail, H. El-Hassan, Development and characterization of fly ash e slag blended geopolymer mortar and lightweight concrete, J. Mater. Civ. Eng. 30 (2018) 1–14, https://doi.org/10.1061/(ASCE)MT.1943-5533.0002209.
[73] S.F.A. Shah, B. Chen, B.S.Y. Oderji, M.A. Haque, M.R. Ahmad, Improvement of early strength of fly ash-slag based one-part alkali activated mortar, Construct. Build. Mater. 246 (2020) 118533, https://doi.org/10.1016/j.conbuildmat.2020.118533.
[74] J. Yuan, P. He, D. Jia, C. Yang, Y. zhang, S. Yan, Z. Yang, X. Duan, S. Wang, Y. Zhou, Effect of curing temperature and $SiO_2/K_2O$ molar ratio on the performance of metakaolin-based geopolymers, Ceram. Int. 42 (14) (2016) 16184–16190, https://doi.org/10.1016/j.ceramint.2016.07.139.
[75] D.M.A. Huiskes, A. Keulen, Q.L. Yu, H.J.H. Brouwers, Design and performance evaluation of ultra-lightweight geopolymer concrete, Mater. Des. 89 (2016) 516–526, https://doi.org/10.1016/j.matdes.2015.09.167.
[76] R.Y. Nkwaju, J.N.Y. Djobo, J.N.F. Nouping, P.W.M. Huisken, J.G.N. Deutou, L. Courard, Iron-rich laterite-bagasse fibers based geopolymer composite: Mechanical, durability and insulating properties, Appl. Clay Sci. 183 (2019) 105333, https://doi.org/10.1016/j.clay.2019.105333.
[77] W.D.A. Rickard, L. Vickers, A. van Riessen, Performance of fibre reinforced, low density metakaolin geopolymers under simulated fire conditions, Appl. Clay Sci. 73 (2013) 71–77, https://doi.org/10.1016/j.clay.2012.10.006.
[78] M. Albitar, M.S.M. Ali, P. Visintin, M. Drechsler, Durability evaluation of geopolymer and conventional concretes, Constr. Build. Mater. 136 (2017) 374–385, https://doi.org/10.1016/j.conbuildmat.2017.01.056.
[79] Z. Pan, K.N. Feng, K. Gong, B. Zou, A.H. Korayem, J. Sanjayan, W.H. Duan, F. Collins, Damping and microstructure of fly ash-based geopolymers, J. Mater. Sci. 48 (8) (2013) 3128–3137, https://doi.org/10.1007/s10853-012-7090-y.
[80] R.T.T. Fongang, J. Pemndje, P.N. Lemougna, U. Chinje-melo, C.P. Nanseu, B. Nait-Ali, E. Kamseu, C. Leonelli, Cleaner production of the lightweight insulating composites: microstructure, pore network and thermal conductivity, Energy Build. 107 (2015) 113–122, https://doi.org/10.1016/j.enbuild.2015.08.009.
[81] J. Feng, R. Zhang, L. Gong, Y. Li, W. Cao, X. Cheng, Development of porous fly ash-based geopolymer with low thermal conductivity, Mater. Dis. 65 (2015) 529–533, https://doi.org/10.1016/j.matdes.2014.09.024.
[82] H.K. Tchakoute, C.H. Rüscher, E. Kamseu, J.N.Y. Djobo, C. Leonelli, The influence of gibbsite in kaolin and the formation of berlinite on the properties of metakaolin-phosphate-based geopolymer cements, Mater. Chem. Phys. 199 (2017) 280–288, https://doi.org/10.1016/j.matchemphys.2017.07.020.
[83] M. Torres-Carrasco, C. Rodríguez-Puertas, M. del M. Alonso, F. Puertas, Alkali activated slag cements using waste glass as alternative activators. Rheological behavior, Bol. Soc. Espanola Ceram. Vidr. 54 (2015) 45-57. 10.1016/j.bsecv.2015.03.004
[84] A.F. Abdalqader, F. Jin, A. Al-Tabbaa, Development of greener alkali-activated cement: utilisation of sodium carbonate for activating slag and fly ash mixtures, J. Clean. Prod. 113 (2016) 66–75, https://doi.org/10.1016/j.jclepro.2015.12.010.
[85] W. Mozgawa, J. Deja, Spectroscopic studies of alkaline activated slag geopolymers, J of Mol. Struct. 924–926 (2009) 434–441, https://doi.org/10.1016/j.molstruc.2008.12.026.
[86] F. Puertas, A. Fernández-Jiménez, Mineralogical and microstructural characterisation of alkali-activated fly ash/slag pastes, Cem. Concr. Comp. 25 (3) (2003) 287–292, https://doi.org/10.1016/S0958-9465(02)00059-8.
[87] H.K. Tchakouté, C.H. Rüscher, Mechanical and microstructural properties of metakaolin-based geopolymer cements from sodium waterglass and phosphoric acid solution as hardeners: a comparative study, Appl. Clay Sci. 140 (2017) 81–87, https://doi.org/10.1016/j.clay.2017.02.002.
[88] K.C. Gomes, G.S.T. Lima, S.M. Torres, S. de Barros, I.F. Vasconcelos, N.P. Barbosa, Iron distribution in geopolymer with ferromagnetic rich precursor, Mater. Sci. Forum 643 (2010) 131–138, https://doi.org/10.4028/www.scientific.net/.
[89] R.I. Iacobescu, V. Cappuyns, T. Geens, L. Kriskova, S. Onisei, P.T. Jones, Y. Pontikes, The influence of curing conditions on the mechanical properties and leaching of inorganic polymers made of fayalitic slag, Front. Chem. Sci. Eng. 11 (3) (2017) 317–327, https://doi.org/10.1007/s11705-017-1622-6.
[90] C.R. Kaze, J.N.Y. Djobo, A. Nana, H.K. Tchakoute, E. Kamseu, U.C. Melo, C. Leonelli, H. Rahier, Effect of silicate modulus on the setting, mechanical strength and microstructure of iron-rich aluminosilicate (laterite) based-geopolymer cured at room temperature, Ceram. Int. 44 (17) (2018) 21442–21450, https://doi.org/10.1016/j.ceramint.2018.08.205.
[91] P.N. Lemougna, K. Wang, Q. Tang, X. Cui, Synthesis and characterization of low temperature (< 800 °C) ceramics from red mud geopolymer precursor, Constr. Build. Mater. 131 (2017) 564–573, https://doi.org/10.1016/j.conbuildmat.2016.11.108.
[92] W.K.W. Lee, J.S.J. van Deventer, Use of infrared spectroscopy to study geopolymerization of heterogeneous amorphous aluminosilicates, Langmuir 19 (21) (2003) 8726–8734, https://doi.org/10.1021/la026127e.

[93] A. Peys, L. Arnout, T. Hertel, R.I. Iacobescu, S. Onisei, L. Kriskova, H. Rahier, B. Blanpain, Y. Pontikes, The use of ATR-FTIR spectroscopy in the analysis of iron-silicate inorganic polymers, n.d. http://slag-valorisation-symposium.eu/2017/wp-content/uploads/downloads/Session%205/Arne%20Peys%20-%20Paper%20-%20The%20use%20of%20ATR-FTIR%20spectroscopy%20in%20the%20analysis%20of%20iron-silicate%20inorganic%20polymers%20-%20SVS2017.pdf , 2017 , (accessed March 5 2021).
[94] S. Zhang, K. Gong, J. Lu, Novel modification method for inorganic geopolymer by using water soluble organic polymers, Mater. Lett. 58 (7–8) (2004) 1292–1296, https://doi.org/10.1016/j.matlet.2003.07.051.
[95] J.G.S. van Jaarsveld, J.S.J. van Deventer, G.C. Lukey, The effect of composition and temperature on the properties of fly ash- and kaolinite-based geopolymers, Chem. Eng. J. 89 (1–3) (2002) 63–73, https://doi.org/10.1016/S1385-8947(02)00025-6.
[96] X. Tian, W. Xu, S. Song, F. Rao, L. Xia, Effects of curing temperature on the compressive strength and microstructure of copper tailing-based geopolymers, Chemosphere 253 (2020) 126754, https://doi.org/10.1016/j.chemosphere.2020.126754.
[97] X. Yao, Z. Zhang, H6. Zhu, Y. Chen, Geopolymerization process of alkali e metakaolinite characterized by isothermal calorimetry, Thermochim. Acta 493 (2009) 49-54. http://dx.doi.org/10.1016/j.tca.2009.04.002.
[98] G. Zhang, J. He, R.P. Gambrell, Synthesis, characterization, and mechanical properties of red mud-based geopolymers, Transport. Res. Rec. 2167 (1) (2010) 1–9, https://doi.org/10.3141/2167-01.
[99] J. He, J. Zhang, Y. Yu, G. Zhang, The strength and microstructure of two geopolymers derived from metakaolin and red mud-fly ash admixture: a comparative study, Construct. Build. Mater. 30 (2012) 80–91, https://doi.org/10.1016/j.conbuildmat.2011.12.011.
[100] Y. Zhang, W. Sun, Q. Chen, L. Chen, Synthesis and heavy metal immobilization behaviors of slag based geopolymer, J. Hazard Mater. 143 (2007) 206–213, https://doi.org/10.1016/j.jhazmat.2006.09.033.
[101] V. Nikolić, M. Komljenović, N. Marjanović, Z. Baščarević, R. Petrović, Lead immobilization by geopolymers based on mechanically activated fly ash, Ceram. Int. 40 (6) (2014) 8479–8488, https://doi.org/10.1016/j.ceramint.2014.01.059.